minerals

MDPI

Article

A Juvenile Component in the Pre- and Post-Collisional Magmatism in the Transition Zone between the Araçuaí and Ribeira Orogens (SE Brazil)

Guilherme Loriato Potratz [1,*], Mauro Cesar Geraldes [2], Edgar Batista de Medeiros Júnior [3], Filipe Altoé Temporim [4] and Maria Virgínia Alves Martins [2,5]

1 Programa de Pós-graduação em Geociências, Faculdade de Geologia, Universidade do Estado do Rio de Janeiro, Rio de Janeiro 20550013, Brazil
2 Departamento de Mineralogia e Petrologia Ígnea, Faculdade de Geologia, Universidade do Estado do Rio de Janeiro, Rio de Janeiro 20550013, Brazil
3 Departamento de Solos, Universidade Federal de Viçosa, Viçosa 36570900, Brazil
4 Faculdade de Ciências e Tecnologia, Universidade Federal de Goiás, Aparecida de Goiânia 74968755, Brazil
5 Departamento de Geociências, GeoBioTec, Universidade de Aveiro, 3810-193 Aveiro, Portugal
* Correspondence: geo.loriato@gmail.com

Abstract: The Araçuaí and Ribeira orogens have been studied for decades, and recently, these two orogens were described as the Araçuaí–Ribeira Orogen System. Despite much work investigating this orogenic system, some issues, such as the connection between the two orogens, are still not fully understood. This work aimed to present unpublished Lu-Hf data for the Santa Angélica Intrusive Complex (SAIC) and for the host rocks that are part of the Rio Negro magmatic arc, as well as to present U-Pb ages for these rocks, thus contributing to the understanding of the geological processes that acted in the transition zone between the Araçuaí and Ribeira orogens. Two samples were collected corresponding to the magmatic arc and six samples from the Santa Angélica Intrusive Complex. The zircon grains were separated from the samples and subjected to geochronological (U-Pb) and isotopic (Lu-Hf) analysis by laser ablation-induced coupled plasma mass spectrometry (LA-ICP-MS). The geochronological data for the host rocks indicate a crystallization age of ca. 595 Ma. In contrast, the Hf isotopic data point to at least two magmatic sources, one crust, and one mantle. The geochronological data obtained for the SAIC rocks show three age peaks. The first peak (537 ± 5 Ma) coincides with the process of crustal anatexis and possibly marks the beginning of the generation of magmas associated with post-collisional magmatism. The second peak (510 ± 5 Ma) registers the apex of crystallization of the SAIC, and the third peak of ages (488 ± 7 Ma) marks the upper limit of the magmatism in the SAIC. The SAIC isotopic data point to at least two crustal components and a mantle component (juvenile).

Keywords: U-Pb geochronology; Lu-Hf isotopes; LA-ICP-MS; magmatism; Mantiqueira Province; Santa Angélica Intrusive Complex

Citation: Potratz, G.L.; Geraldes, M.C.; Medeiros Júnior, E.B.d.; Temporim, F.A.; Martins, M.V.A. A Juvenile Component in the Pre- and Post-Collisional Magmatism in the Transition Zone between the Araçuaí and Ribeira Orogens (SE Brazil). *Minerals* **2022**, *12*, 1378. https://doi.org/10.3390/min12111378

Academic Editor: José Javier Alvaro

Received: 20 September 2022
Accepted: 25 October 2022
Published: 29 October 2022

1. Introduction

The segment located between parallels 17° S and 25° S along the east coast of Brazil comprises two contiguous orogenic components: the Ribeira orogen, in which transpressional tectonics predominate, and the Araçuaí orogen, characterized by crustal shortening and its confined development [1,2]. This crustal segment, named the Araçuaí–Ribeira Orogenic System (AROS), is marked by intense orogenic magmatism that develops between ca. 850 Ma and ca. 480 Ma and in the different stages of evolution of the AROS components (pre-, syn-, late- and post-collisional) [3–7]. Despite extensive work carried out both in the Araçuaí orogen segment and in the Ribeira orogen segment, the transition zone between the orogens is still a matter of discussion since the only known link is the Rio Doce magmatic arc [3,7,8].

For many years the 21° S parallel was used as a reference to limit the two crustal segments (Araçuaí and Ribeira) [4,5,9]. However, the structural data of those orogens demonstrate a gradual transition in the tectonic style between the orogens, where the Araçuaí orogen presents foreland-directed thrusts and an anatectic metamorphic core, and the Ribeira orogen is characterized by a broad set of NE–SW direction shear zones. [1]. In addition to structural data, the detailed study of pre-collisional batholiths and plutons (ca. 630 Ma to ca. 585 Ma) of the transition zone between the orogens demonstrates some continuity between the orogens [3,7,8]. Finally, the igneous bodies associated with the AROS collapse (ca. 530 Ma to ca. 480 Ma) show a significant difference between the Araçuaí and Ribeira orogens [10,11].

The post-collisional magmatism that develops in the Ribeira orogen is essentially granitic, with restricted cases of intermediate and basic rocks [11,12]. In the Ribeira orogen, the post-collision bodies are grouped into I-type granites, represented by the Suruí and Nova Friburgo suites, and S-type granites, represented by the Sana suite [11–13]. In the Araçuaí orogen, the magmatism associated with the collapse of the orogen presents greater complexity, subdivided into the G4 and G5 super suits [5]. The G4 super suite is limited to the northern segment of the Araçuaí orogen, composed essentially of S-type granites [5]. The G5 super suite is composed of intrusive complexes whose main characteristic is bimodal magmatism, with magmas of the mantle and crustal origin [10,14]. Still, in the Araçuaí belt segment, the post-collisional bodies of the southern part are relatively small, with balloon shapes and inverse zoning. In contrast, the igneous bodies of the northern piece are represented by much larger batholiths consisting of granitoids and charnockites [15].

The main representative of the G5 super suite is the Santa Angélica Intrusive Complex (SAIC), a relatively small intrusion (200 km^2) located in the transition zone between the Araçuaí and Ribeira orogens [14]. What makes the SAIC one of the main representatives of the G5 super suite is its inversely zoned relief, the complexity of igneous facies existing in this unit, the diversity of features that are typical of magma mixing processes, and consequently, the number of works that have been developed at the SAIC since the 1980s [14–25].

Despite decades of work at the SAIC and other igneous units related to the AROS collapse, much remains to be done to understand the post-collisional magmatism of this region, not only from a structural and geochronological point of view, but also from the processes of generation of magmas, magmatic differentiation, and the different crustal levels of placement of those igneous bodies [10]. One of the gaps still open about the SAIC and most of the units of the G5 super suite is the determination of the isotopic signature of the mantle sources that are present in this suite since the isotopic data of the Sm-Nd and Rb-Sr systems in total rock indicated only the presence of a crustal component [10,14]. Therefore, this work aims to present isotopic data of the Lu-Hf system for the SAIC rocks to contribute to understanding the different magmatic sources of the SAIC and present U-Pb ages in zircon grains for the different igneous facies of the SAIC. Finally, this work also presents geochronological (U-Pb) and isotopic (Lu-Hf) data for the host rocks of the SAIC, which represent the Rio Doce magmatic arc, thus contributing to the evolution of knowledge about the connection between the Araçuaí and Ribeira orogens.

2. Geological Setting

The Santa Angélica Intrusive Complex (SAIC) is in the southern region of the state of Espírito Santo (SE—Brazil), between the municipalities of Alegre, Castelo, and Cachoeiro do Itapemirim. This region is in the zone on the southern edge of the Araçuaí orogen, which connects with the Ribeira orogen (Figure 1) [8,10,14]. The Araçuaí orogen and its African counterpart represent an orogen of confined origin, limited by the São Francisco-Congo Craton on its eastern, northern, and western edges [5,26]. In contrast, the Ribeira orogen represents a more complex orogenic system, including two systems of magmatic arcs and their related basins, which were added in multiple episodes of collision, with its apex in the collision of the Cabo Frio Terrain, corresponding to a portion of the Angolan base [27–30].

For decades, the correlation between the Araçuaí and Ribeira orogens was somewhat complex since they were described and subdivided based on different methodologies and considered very different sectors of the geotectonic scenario, lithotectonic components, and development time [9,31]. With the development of studies on the magmatic arcs of the two orogens and the detailed geological mapping of the transition zone between the orogens, the designation of the Araçuaí–Ribeira Orogenic System (AROS) was proposed [32]. The AROS was subdivided into five tectonic domains: (i) Araçuaí Belt Domain; (ii) Domain of the Rio Doce Arc; (iii) Domain of the Rio Negro Arc; (iv) Cabo Frio Domain; and (v) Southern Ribeira Belt.

The SAIC is in the Rio Doce Arc domain, which represents the upper plate of the subduction process and is represented by the Rio Doce magmatic arc, the basins related to the arc, and the Rhyacian–Orosian basement [32] (Figure 1). The Rio Doce Magmatic Arc is composed of the plutonic rocks and metavolcanic sedimentary successions of the Rio Doce group, whose lithogeochemical and isotopic dataset points to a magmatic arc formed essentially in a continental margin tectonic configuration, around 630 to 580 Ma [5,7,33,34].

The basement of the Rio Doce Arc domain is represented by the Quirino, Juiz de Fora, and Pocrane complexes of the Rhyacian–Orosian age [35,36]. In the fore-arc region of the Rio Doce Arc domain, large areas of the Rhyacian–Orosian basement, Neoproterozoic paragneisses, and syn-collisional granites (ca. 580 Ma to ca. 535 Ma) stand out [32,35]. In the back-arc region of the Rio Doce Arc domain, high-grade metamorphic paragneisses, syn- to late-collisional granites (suites G2 and G3), and the intrusions of the G5 super suite, where the CISA is located, stand out [10,37,38].

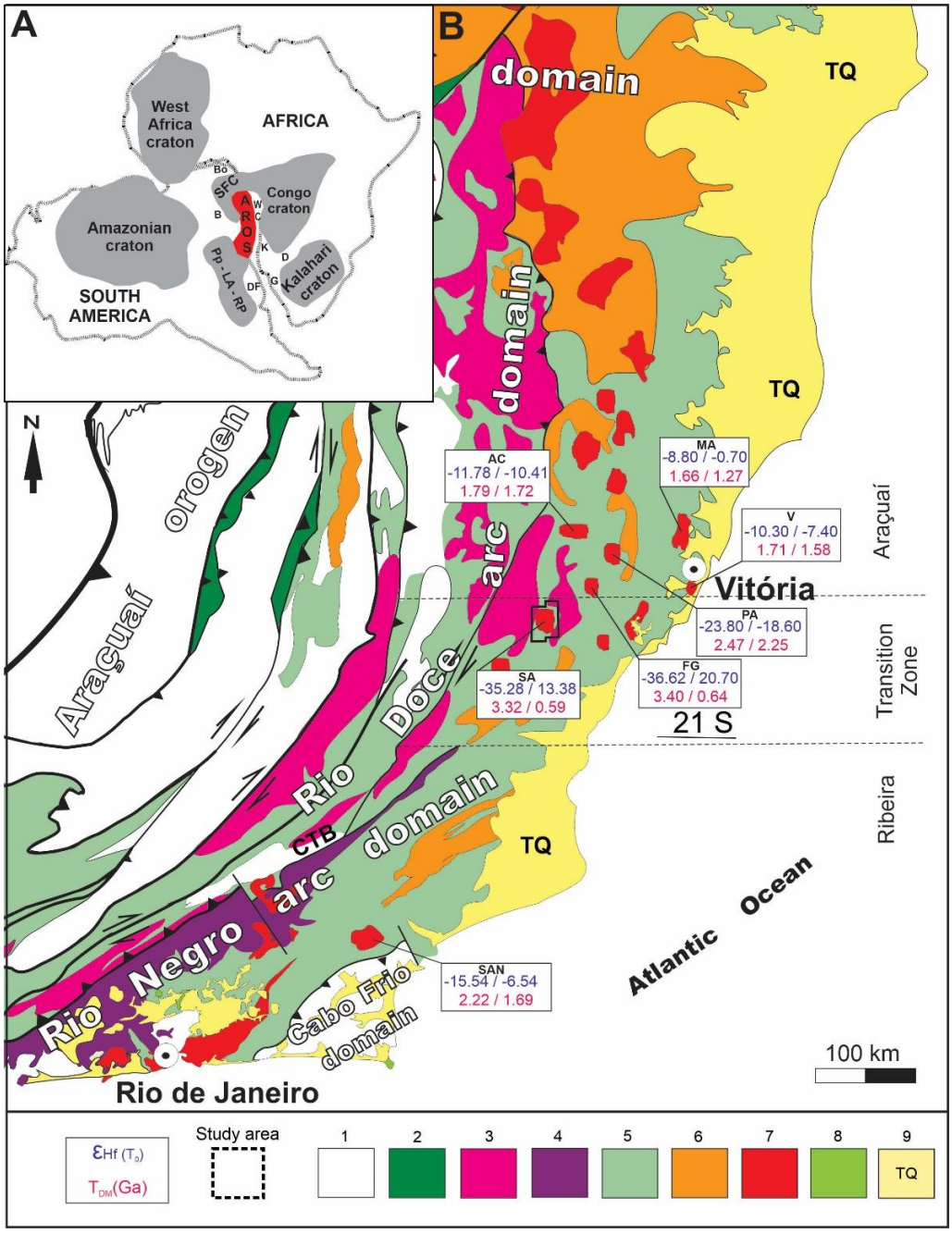

Figure 1. (**A**) Location of the Araçuaí-Ribeira Orogenic System (AROS) in Western Gondwana and the position of the Brasiliano Pan African orogenic belts: B—Brasília; Bo-Borborema; D-Damara; DF-Dom Feliciano; G-Gariep; K-Kaoko; WC-West Congo, and cratons SFC-São Francisco; Pp-LA-RP-Paranapanema-Luís Alves-Rio de La Plata. (**B**) Simplified geological map of AROS adapted from [7,8,32]. Legend: AC-Afonso Cláudio Intrusive Complex; SA-Santa Angélica Intrusive Complex; MA-Mestre Álvaro Massif; V-Vitória Massif; PA-Pedra Azul-Arecê Intrusive Complex; FG-Forno Grande Intrusive Complex; SAN-Sana granite. LEGEND: 1-Pre-Neoproterozoic units; 2-Neoproterozoic ophiolite-bearing rock assemblages; 3-batholiths and stocks of the Rio Doce magmatic arc (ca. 630–585 Ma) and probable correlatives; 4-Rio Negro-Serra da Prata arc domain (Rio Negro and Serra da Prata magmatic arcs and related units; ca. 860–630 Ma); 5-Neoproterozoic metasedimentary and metavulcanic successions; 6-granitic collisional rocks (ca. 590–535 Ma); 7-post-collisional intrusions (ca. 525–470 Ma); 8-Cenozoic Alkaline magmatism; 9-Cenozoic cover (TQ); CTB: Central Tectonic Boundary. The Lu-Hf isotopic data presented in the figure were obtained in this work [31,34,39–41].

3. The Santa Angelica Intrusive Complex

The SAIC is intruded in the rocks of the Rio Doce magmatic arc, represented in the region by the Muniz Freire orthogneiss and by the paragneisses of the Bom Jesus do Itabapoana group (Figure 2). The contact between the country rocks and the CISA is sub-vertical. The foliation of the country rocks is parallel to the edges of the CISA, plunging with angles greater than 50° toward the intrusion [16]. The Muniz Freire orthogneiss unit is predominantly formed by metagranites, with localized variations of metagranodiorites, matetonalites, and metadiorites [23,42,43]. The crystallization age obtained for the metagranite from the Muniz Freire unit is 590 +2/−4 Ma (U-Pb in zircon) [20]. In the Bom Jesus do Itabapoana group, the predominant rock is orthopyroxene–garnet–biotite gneiss, and the unit presents a high degree of migmatization. The age for the maximum deposition limit of the sediments that gave rise to the Bom Jesus do Itabapoana group is 666 ± 1 Ma, and the age of metamorphism of the rocks of this unit is ca. 600 Ma [44].

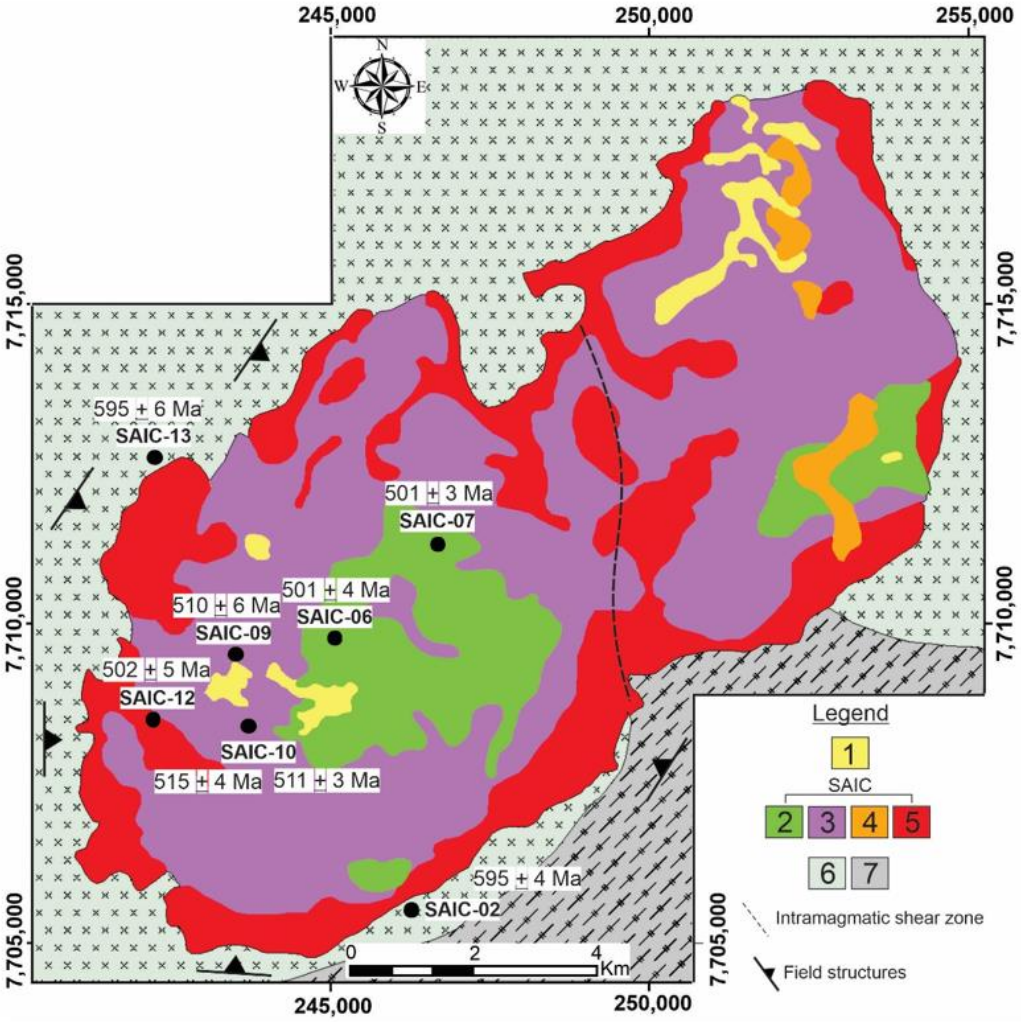

Figure 2. Geological map of the Santa Angélica Intrusive Complex (SAIC). Legend: (1) Cenozoic sediments; (2) Gabbro/Norite; (3) Hybrid Zone; (4) Granite type 2; (5) Granite type 1; (6) Orthogneiss Muniz Freire; and (7) Paragneisse Bom Jesus do Itabapoana. The points plotted on the map represent the locations (in outcrops) where the SAIC samples studied in this work were collected. Source: Adapted from [21]. The presented U-Pb ages were obtained in this work.

The SAIC (Figure 2) is composed of a complex set of mafic, intermediate, and felsic rocks. The mafic rocks found in the SAIC are gabbronorite, quartz diorite and leucopyroxene-hornblend gabbro [17,45,46]. Among the felsic rocks, porphyritic granites with abundant allanite, called type-1 granites, and fine- to medium-grained granites with titanite

as the dominant accessory phase, called granites type 2, stand out [17]. In the group called granites type 1, syenogranites, monzogranites, quartz syenites, and quartz monzonites are found, while the group of granites type 2 is restricted to syenogranites [23].

The intermediate rocks of the SAIC, mostly granodiorites, are present in what has been called the hybrid zone. This hybrid zone is characterized by features typical of magma mixing processes, making it challenging to map the rocks in that zone. The main features of magma mixing observed at the outcrop and hand sample levels are microgranular enclaves of varied composition, fine-grained gabbroic lenses with rounded K-feldspar and quartz xenocrystals and lattice–vein complexes. The SAIC rocks also exhibit microscopic features associated with the mixing process of magmas, such as acicular crystals of apatite, maintained textures like hornblende-mantled biotites, quartz, and K-feldspar inclusions in mafic minerals [16,23,45,46].

The felsic rocks occur mainly on the edges of the SAIC. In contrast, the mafic rocks are concentrated in the center of the intrusion, which gives the SAIC a geomorphological feature called inversely zoned relief, where the edges of the intrusion are higher than its scepter [45]. The SAIC also presents an intramagmatic shear zone, observed in the field and through magnetic anisotropy surveys, which separate the intrusive complex into two lobes (SW and NE) [17,18,25]. Finally, a series of microstructural features observed in the SAIC rocks demonstrate processes of submagmatic deformation, which are associated with the turbulent flow of magmas and the difference in viscosity of the magmas that gave rise to the SAIC [22,24].

The geochemical signature of the SAIC indicates an expanded subalkaline to slightly alkaline series and anomalous potassium values [19]. The $^{87}Sr/^{86}Sr$ ratios for mafic rocks vary from 0.707 to 0.709 [20]. The epsilon Nd values are very low for the SAIC rocks. For Gabbronorite, the εNd is -19.76; for allanite granite (granite type 1), the εNd value is -20.74 [10].

Magnetic anisotropy studies demonstrated a strongly anisotropic pattern in the SAIC, in which both lineation and magnetic foliation show a concentric way around the two mafic cores [25]. In the NE lobe, the magnetic lineation is practically vertical (dips between 61° and 90°), while in the SW lobe, the magnetic lineation presents a low angle (dips between 0 and 29°) [25].

4. Materials and Methods

Two field campaigns were conducted for the reconnaissance of the SAIC, a description of the rocks and their macroscopic features, and sample collection for U-Pb geochronology and Lu-Hf isotopic analysis. Overall, seven sampling locations were visited, two outcrops of country rocks from the Santa Angelica Intrusive Complex and the remaining six samples from the SAIC. The sampling locations are shown on the geological map in Figure 2. The slides for petrographic analysis were prepared in the Geological Sample Preparation Laboratory (LGPA) of the Universidade do Estado do Rio de Janeiro (UERJ). The thin slides were described at the Petrography Laboratory at UERJ.

The samples collected from the Santa Angelica Intrusive Complex were separated into three groups according to their field and petrographic characteristics: (1) holo leucocratic/leucocratic rocks, (2) melanocratic rocks, and (3) hybrid rocks. The hybrid rock group was subdivided into granitic and gabbroic rocks. All outcrops in the hybrid rock group were considered since the predominant lithology could not be determined, and no apparent features of magma mixing processes were observed.

For determination of the U-Pb ages and the isotopic geology of the Lu-Hf system, two samples of the SAIC country rocks (SAIC-02 and -13) and six samples representing the SAIC (SAIC-06.A, -07.A, -09, -10.A, -10.B, and -12) were selected. Of the six samples, one corresponds to the leucocratic rock group (no magma mixing features), one sample from the melanocratic rock group, two samples from the granitic portion of the hybrid rock group, and two samples of gabbro from the hybrid rock group. The detailed procedure for preparing the samples and separating the zircon grains is presented in detail in

SM.A. The characterization of the zircon grains was based on the work of Corfu and its collaborators [47].

To determine U-Pb ages, analyses were performed at the Multi-user Laboratory for Environment and Materials (MultiLab) at UERJ using a Laser Ablation Induction Coupled Plasma Mass Spectrometer (Thermo Neptune Plus; LA-ICP-MS). The isotopic ratios of the zircon grains were determined using multiple collectors. The sequence of readings occurred in a specific order: (1) read from the blank, (2) read from the GJ-1 standard zircon, (3) read from the sequence of nine unknown zircon grains, (4) read from the 91,500-standard zircon, (5) read from the GJ-1 standard zircon, and (6) read from the blank. The data were transferred to an Excel spreadsheet on which they were analyzed.

In the laser ablation (LA) methodology, a high-power beam and laser were used to vaporize the material from the grain surface. Upon coupling to the inductively coupled plasma/mass spectrometry (ICP/MS), the vapor was transported via a He stream to the plasma in which the atoms were ionized, and isotope ratio measurements were obtained from the spectrometer. The ICP/MS multi-collector contains nine Faraday cups and seven compact discrete dynode ion counters (CDD). The U–Th–Pb analyses included measurements of ^{204}Pb, ^{206}Pb, ^{207}Pb, ^{208}Pb, ^{232}Th, and ^{238}U masses. Hg represents a common contaminant in He and Ar gases. ^{204}Hg interferes with mass counts of ^{204}Pb. The ^{202}Hg, the mass 204 (^{204}Pb + ^{204}Hg), and the isotopes ^{206}Pb, ^{207}Pb, and ^{208}Pb were detected using ion counters, while 238U and 232Th were measured with day glasses. Laser-ablated material was transported in Ar (0.80 L/min) and He (0.55 L/min) for analyses using 40 cycles of 1.045 s each.

The zircon samples from this work were analyzed in conjunction with international zircon standards GJ-1 (TIMS normalization data ^{207}Pb/^{206}Pb = 608.3 Ma, ^{206}Pb/^{238}U = 600.7 Ma, and ^{207}Pb/^{235}U = 602.2 Ma [48] and 91,500 (ID-TIMS ages for ^{206}Pb/^{238}U = 1062.4 ± 0.8 Ma and ^{207}Pb/^{206}Pb = 1065.4 ± 0.6 Ma) following the sequence of one blank, one standard, nine unknown samples, one blank, and two standards. The GJ-1 zircon standard for a 30 µm ablation point yielded several pieces of data: (1) 432,000–114,000 cps of ^{206}Pb, (2) 25,000–7000 cps of ^{207}Pb, (3) 6500–4200 cps of ^{208}Pb, (4) 4400–4200 cps of ^{202}Hg, and (5) 1060–1090 cps mass of 204 (^{204}Pb + ^{204}Hg). For ^{232}Th and ^{238}U measurements in Faraday cups, the values were 0.78 and 6.06 mV, respectively, yielding an age of 603 ± 5.7 Ma. An Excel spreadsheet performed offline corrections for the blank, Hg interference, and ordinary Pb. The values obtained for the GJ-1 standard zircon were compared with accepted values [48] to calculate a conversion factor applied to the nine unknown samples. Finally, the ISOPLOT program (version 4.1.5) was used to calculate ages and construct Concordia diagrams [49].

Lu-Hf analyses were performed with a 50 µm spot at the locations from which the U–Pb analyses were obtained. The data acquisition sequence contained 50 cycles, starting with a blank reading, and reading the GJ-1 zircon and Mud Tank standards. After those readings were obtained, 10 grains of unknown samples were analyzed, finishing with the analyses of zircon standards 91,500 and GJ-1 and one more blank reading. Alves and collaborators describe the analytical procedure adopted for the Lu-Hf analyses in detail [50]. Complementary information about the Lu-Hf methodology is presented in Supplementary Material.

For the calculation of ages, only the spots that presented discordance ≤ 5% (in modulus), the fraction of ^{206}Pb/^{204}Pb ≤ 0.005, Th/U ratio > 0.19, individual errors of the ratios ≤ 8% and Rho values > 30% were considered. For the Lu-Hf analyses, only those with error < 1.0 (±2 SD) and TDM model ages greater than the crystallization ages of the respective samples were considered.

5. Results

5.1. Sample SAIC-02.A

The SAIC-02.A sample was collected from the outcrop region of the Muniz Freire orthogneiss (Figure 2) at the SE edge of the SAIC. The metagranitoid from that region was light gray, medium to coarse-grained, with a granolepidoblastic texture and poorly devel-

oped foliation (Figure 3A). The rock was essentially composed of microcline, plagioclase, biotite, and quartz, with zircon, allanite, and apatite as accessory minerals.

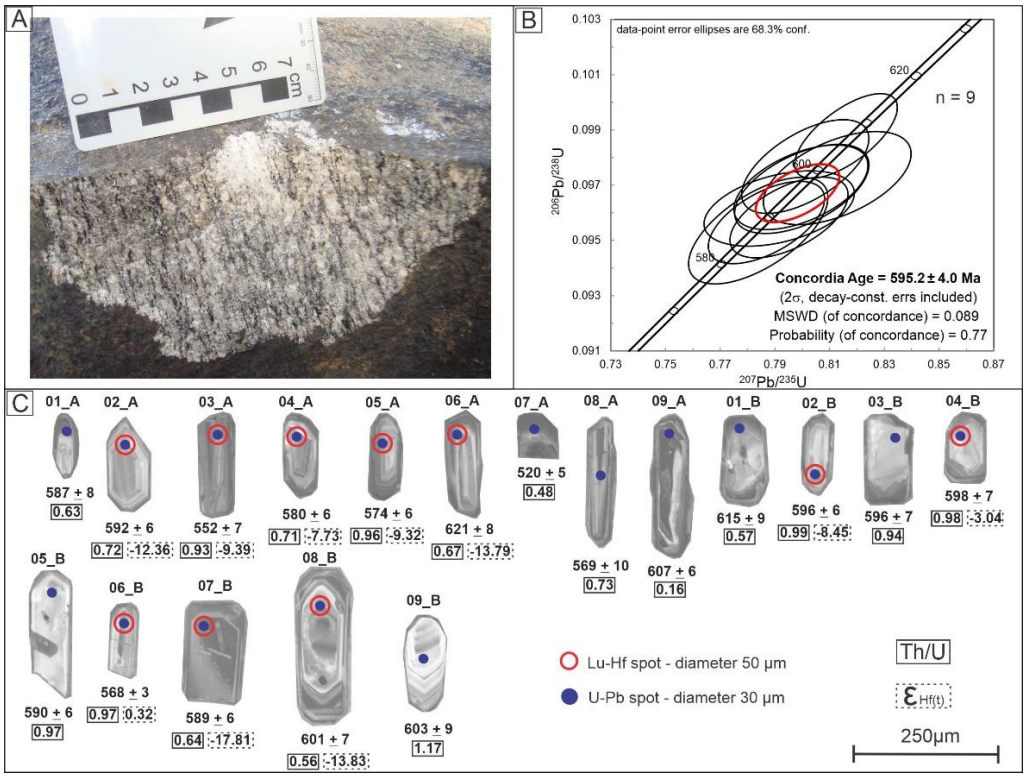

Figure 3. (**A**) Representative sample of Muniz Freire orthogneiss from the point SAIC-02. (**B**) Concord age for the sample SAIC-02.A. (**C**) Cathodoluminescence image of the analyzed zircon grains.

The zircon crystals in this sample are euhedral and show prismatic habit with length-to-width ratios of 4:1, 3:1, and 2:1 (Figure 3C). The crystals show narrow and well-developed growth zonation with homogeneous cores, except grain 08-B (Figure 3C), which has a xenocryst core. Twelve grains, whose Th/U ratio ranged from 0.16 to 0.99, were used to determine the age of this sample (Supplementary Material). The calculated Concordia age for sample SAIC-02 was 595 ± 4 Ma with mean square weighted deviation (MSWD) = 0.089 and probability = 0.77 (Figure 3B).

Complete Lu-Hf data are presented in Supplementary Material. Analyses were obtained on 10 zircon grains, and no data were discarded from this sample. Model ages for the depleted mantle ranged from 2.6 to 1.4 Ga, and εHf values ranged from −18.01 to 0.30.

5.2. Sample SAIC-13

This sample was collected at the NW edge of the SAIC, also in the outcrop area of the Muniz Freire orthogneiss (Figure 2). The metagranitoid has a light gray to yellowish color, medium- to coarse-grained, granoblastic to lepidoblastic texture, and protomylonite pattern (Figure 4A). The rock is essentially composed of microcline, plagioclase, biotite, and quartz, with zircon and apatite as accessory minerals.

The zircon crystals in this sample are euhedral and exhibit prismatic habit with length-to-width ratios of 3:1 and 2:1 (Figure 4C). The crystals exhibit narrow, well-developed growth zonation with homogeneous cores. Nine grains, whose Th/U ratio ranged from 0.66 to 1.33, were used to determine the age of this sample (SM.C). The calculated Concordia age for the sample SAIC-13 was 595 ± 6 Ma, with MSWD = 0.073 and probability = 0.73 (Figure 5B).

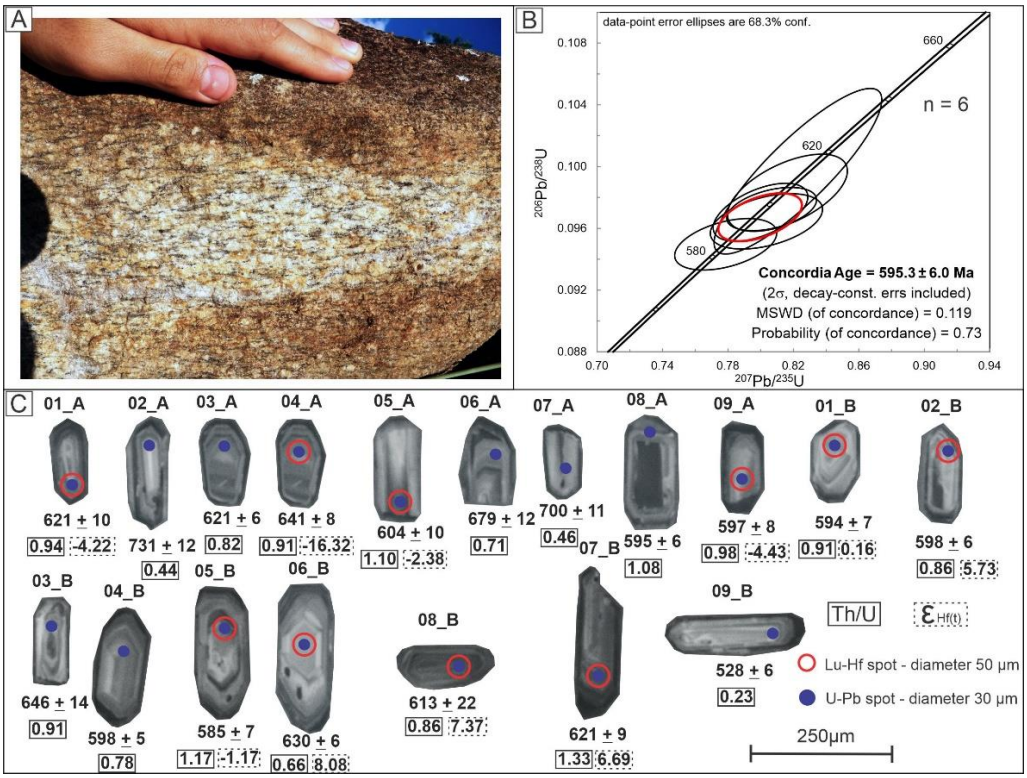

Figure 4. (**A**) Representative sample of Muniz Freire orthogneiss from the point SAIC-13. (**B**) Concord age for the sample SAIC-13. (**C**) Cathodoluminescence image of the analyzed zircon grains.

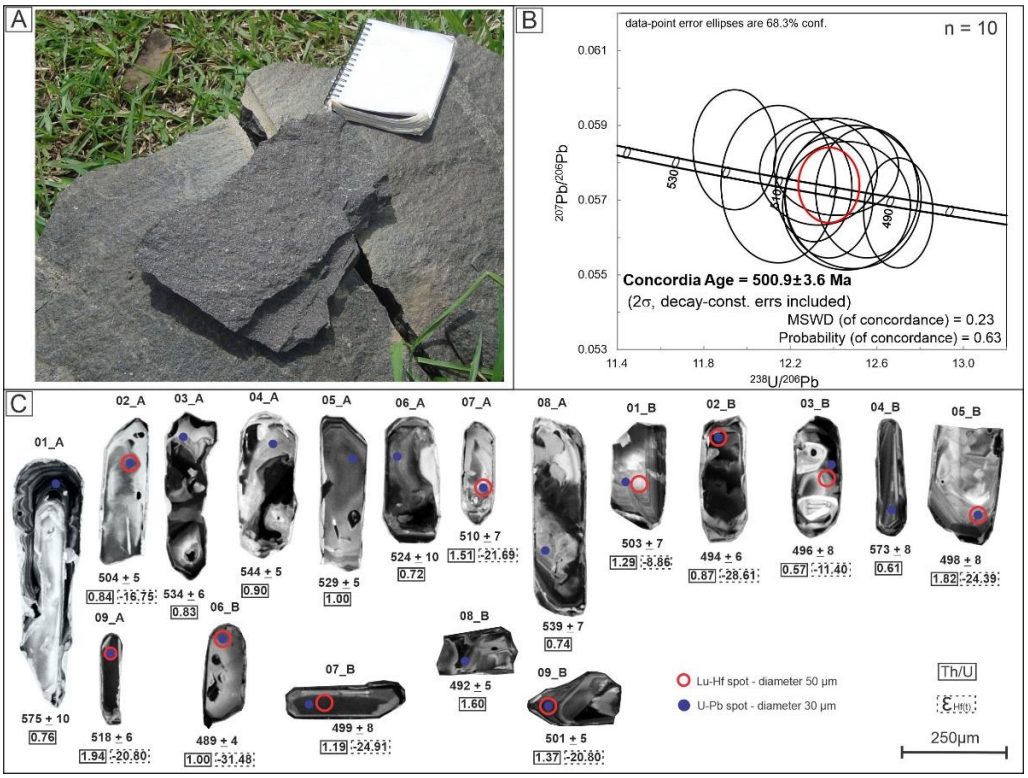

Figure 5. (**A**) A representative sample of SAIC mafic core from the point SAIC-06. (**B**) Concord age for the sample SAIC-06A. (**C**) Cathodoluminescence image of the analyzed zircon grains.

Complete Lu-Hf data are presented in SM.D. Analyses were obtained on 10 zircon grains, and no data from this sample was discarded. Model ages for the depleted mantle ranged from 2.37 to 0.99 Ga, and εHf values ranged from −6.32 to 8.08.

5.3. Sample SAIC-06.A

Sample SAIC-06.A was collected in the NE lobe's mafic core (Figure 2). It is a melanocratic rock with equigranular texture, fine to medium-grained, and classified as a gabbronorite (Figure 5A). This rock had plagioclase, biotite, hornblende, and augite as essential minerals, with hypersthene, titanite, opaque minerals, and zircon as accessory minerals. On a thin slide, the rock showed a porphyritic texture. Coronas of hornblende frequently occurs in rounded biotite crystals.

The zircon population from this sample showed a prismatic habit, generally elongated, with length-to-width ratios of 4:1, 3:1, and 2:1 (Figure 5C). Some crystals, such as grain 01-A (Figure 5B), show textural discontinuities along the growth zonation. In general, the crystal zoning is distant and often develops near the edges of the crystals. Grains 03. A and 03. B (Figure 5B) have xenocryst cores. Analyses of 10 zircon grains (SM.C) with Th/U ratios ranging from 0.57 to 1.94 were used to determine the crystallization age of this sample. The estimated Concordia age for the sample was 501 ± 4 Ma with MSWD = 0.23 and a probability = 0.63 (Figure 5B).

For isotopic data, eight analyses were used for this sample, and two were discarded from the interpretations because they were outside the quality standards adopted in this work. Model ages for the depleted mantle ranged from 3.09 to 1.83 Ga, and εHf values ranged from −31.45 to −8.46.

5.4. Sample SAIC-07.A

This sample was also collected from the NE lobe's mafic core. It is a melanocratic rock with an inequigranular porphyritic texture and a fine- to medium-grained matrix. The K-feldspar xenocrystals are rounded and can reach up to 5 cm (Figure 6A). The rock matrix, classified as quartz diorite, was composed of plagioclase, biotite, augite, and hypersthene and contained quartz, orthoclase, apatite, opaque minerals, and zircon as an accessory mineral. On a thin slide, the rock matrix showed subophitic texture, inclusions of quartz and orthoclase in biotite and augite, and acicular apatite crystals.

This sample has a heterogeneous population of zircon crystals (Figure 6C) with prismatic and granular habits. The prismatic crystals are euhedral to subhedral, and the length-to-width ratio is 4:1, 3:1, and 2:1 (Figure 6C). The cores are generally homogeneous, and growth zonation occurs incipiently near the grain edges. The crystallization age was calculated from the analytical results of 16 grains showing Th/U ratios ranging from 1.21 to 2.43 (SM.C). The estimated Concordia age for the sample is 501 ± 3 Ma with MSWD = 0.0083 and probability = 0.93 (Figure 6B). For the isotopic data, 10 analyses were used for this sample. Model ages for the depleted mantle ranged from 3.09 to 0.64 Ga, and εHf values ranged from -31.34 to 12.44 (SM.D).

5.5. Sample SAIC-09

Sample SAIC-09 was collected in the hybrid zone (Figure 2). It is a melanocratic rock with fine to coarse-grained inequigranular texture and quartz veins scattered throughout it (Figure 7A). This sample was classified as quartz diorite with plagioclase, biotite, hornblende, and augite as essential minerals and quartz, orthoclase, hypersthene, apatite, opaque minerals, and zircon as accessory minerals. The rock showed subophitic texture on thin slides, apatite crystals with an acicular habit, coronas of hornblende in biotite crystals, and augite crystals with quartz and orthoclase inclusions.

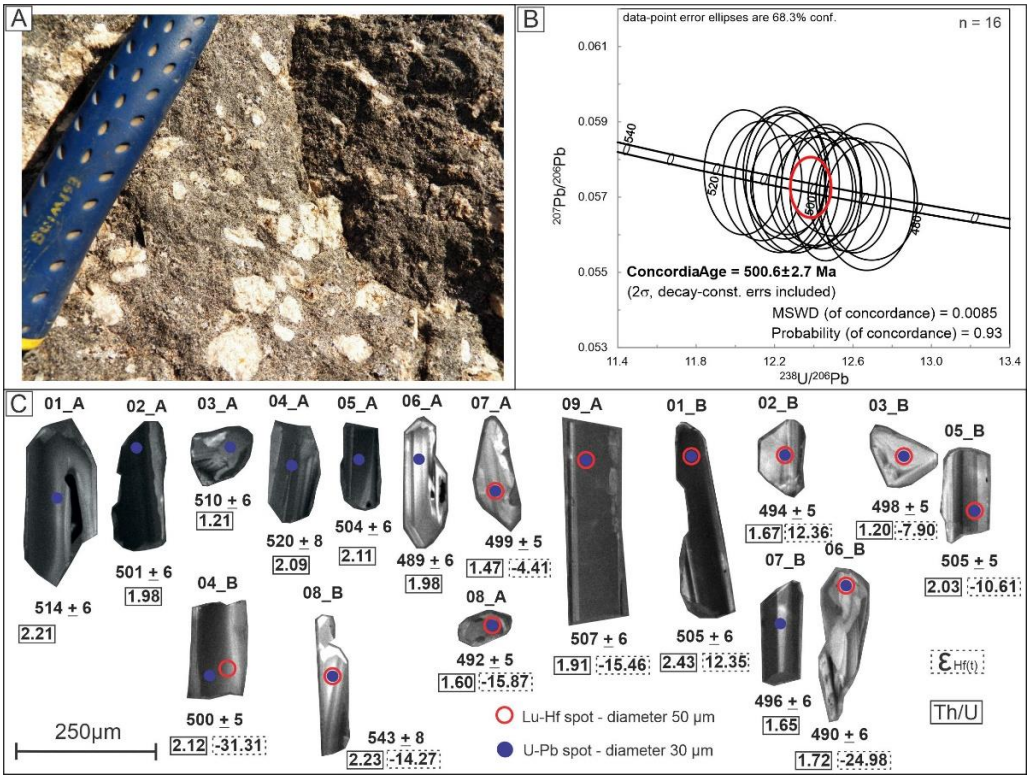

Figure 6. (**A**) A representative sample of the SAIC hybrid rock from the point SAIC-07. (**B**) Concord age for the sample SAIC-07A. (**C**) Cathodoluminescence image of the analyzed zircon grains.

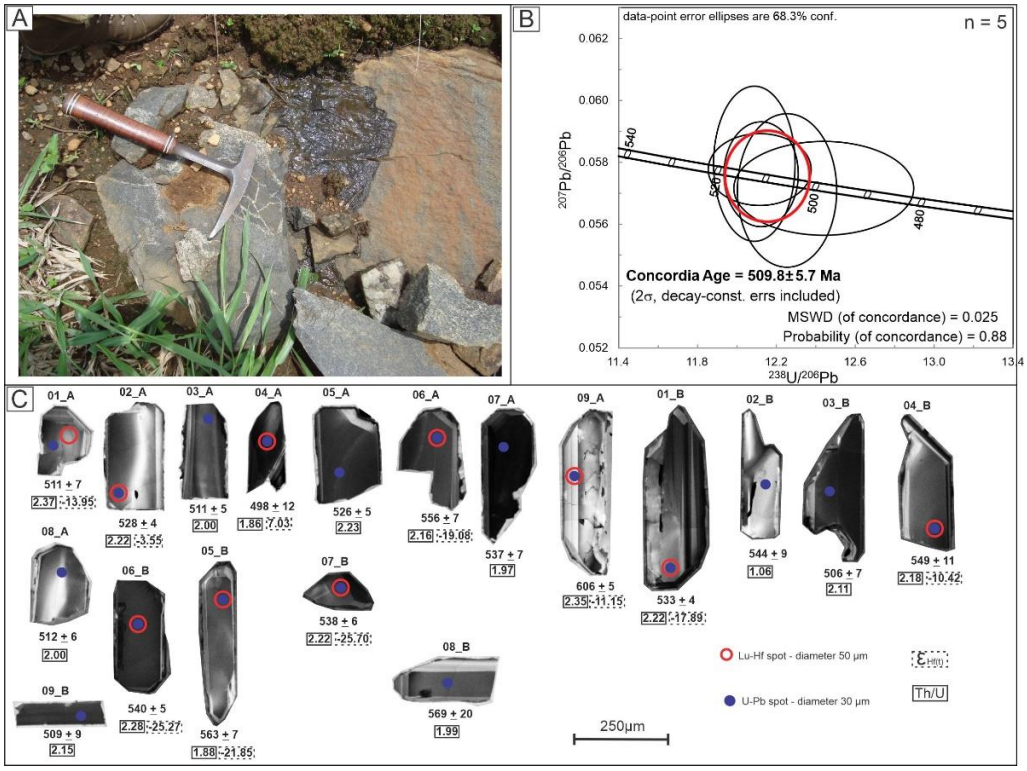

Figure 7. (**A**) A representative sample of the SAIC hybrid rock from the point SAIC-09. (**B**) Concord age for the sample SAIC-09. (**C**) Cathodoluminescence image of the analyzed zircon grains.

The zircon grain population shows an elongate prismatic habit with length-to-width ratios of 5:1, 4:1, 3:1, and 2:1 (Figure 7C). The crystals have homogeneous cores with tightly

spaced growth zoning at the grain edges. Textural discontinuities in the growth zoning are sometimes observed. The crystallization age was calculated from the analytical results of five grains with Th/U ratios ranging from 1.86 to 2.37 (SM.C). The determined Concordia age for the sample was 510 ± 6 Ma with MSWD = 0.025 and probability = 0.88 (Figure 7B). In terms of isotopic data, 10 analyses were used for this sample. Model ages for the depleted mantle ranged from 2.77 to 0.95 Ga, and εHf values ranged from −25.08 to 6.77 (SM.D).

5.6. Sample SAIC-12

Sample SAIC-12 was collected from the outcrop area of the granite type 1 (Figure 2). It is a leucocratic, inequigranular, fine- to medium-grained rock (Figure 8A). This rock is classified as alkali-feldspar granite and contains quartz and orthoclase as essential minerals, and the accessory minerals are biotite, plagioclase, allanite, opaque minerals, and zircon.

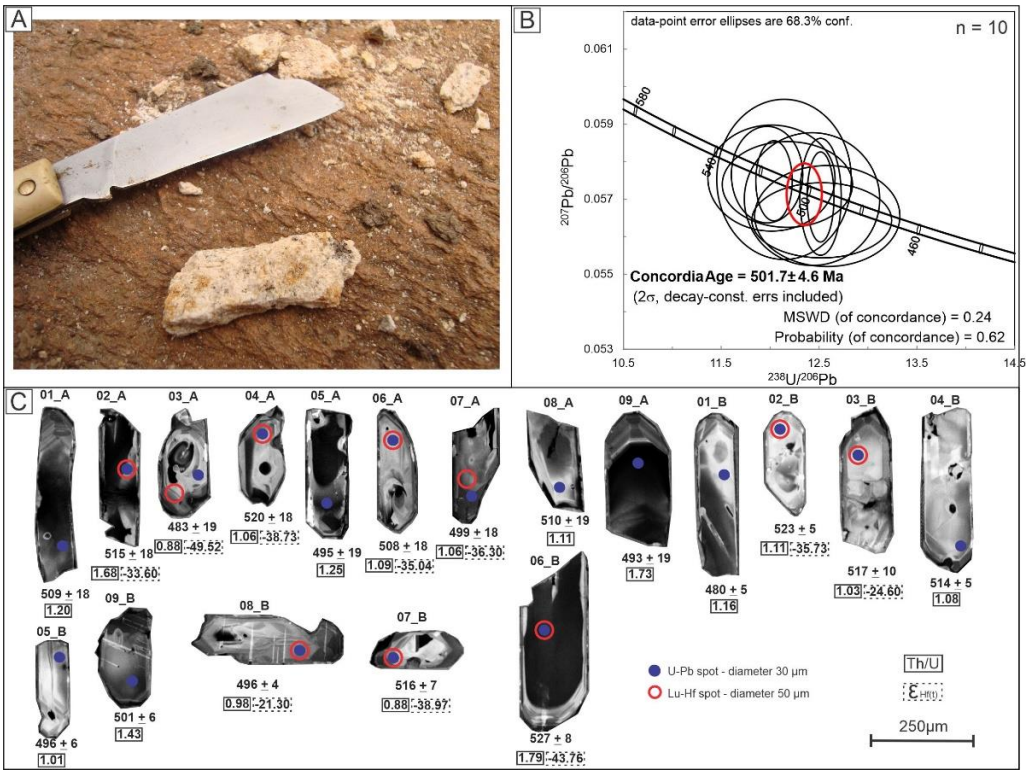

Figure 8. (**A**) A representative sample of SAIC granite type 1 from the point SAIC-12. (**B**) Concord age for the sample SAIC-12. (**C**) Cathodoluminescence image of the analyzed zircon grains.

The zircon grain population of this sample had an elongated prismatic habit with length-to-width ratios of 4:1, 3:1, and 2:1 (Figure 8C). Grains 03.A and 09.B had xenocryst cores with growth directions different from the rest of the grain. The crystal growth zoning is narrow, and some cases could observe textural discontinuities. Analyses of 10 zircon grains (SM.C), with Th/U ratios ranging from 0.88 to 1.73, were used to determine the crystallization age of this sample. The calculated Concordia age for the sample was 502 ± 5 Ma, with MSWD = 0.24 and probability = 0.62 (Figure 8B).

Only two analyses were used for the isotopic data for this sample, and the others were discarded from the interpretations because they were outside the quality standards adopted in this work. Model ages for the depleted mantle ranged from 3.32 to 2.71 Ga, and εHf ranged from −35.28 to −24.25.

5.7. Sample SAIC-10.A

This sample was collected in the SAIC hybrid zone (Figure 2). It is a mesocratic and fine- to coarse-grained rock with an inequigranular texture (Figure 9A). In the hand

sample, it was possible to observe alkali-feldspar crystals surrounded by biotite and opaque minerals. The rock, classified as monzogranite, is composed of orthoclase, plagioclase, quartz, biotite, titanite, allanite, apatite, opaque minerals, and zircon as accessory minerals. On a thin slide, apatite crystals with acicular habit and biotite crystals with inclusions of rounded orthoclase and quartz crystals were often observed.

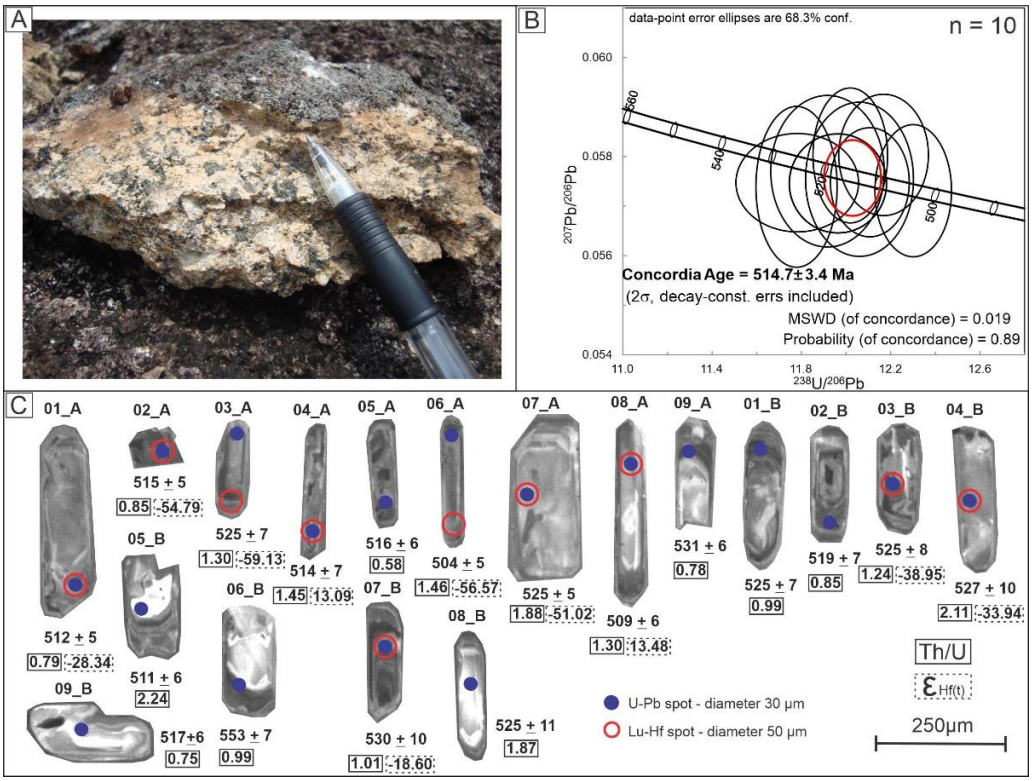

Figure 9. (**A**) A representative sample of the SAIC felsic hybrid rock from the point SAIC-10. (**B**) Concord age for the sample SAIC-10A. (**C**) Cathodoluminescence image of the analyzed zircon grains.

The zircon grains in this sample had elongated prismatic habits with length-to-width ratios of 6:1, 5:1, 4:1, 3:1, and 2:1 (Figure 9C). Grain 06-B had a xenocryst core with a growth direction distinct from the rest of the grain. The crystal growth zoning was narrow, and sometimes, textural discontinuities occurred. Analyses of 10 zircon grains (SM.C), with Th/U ratios ranging from 0.75 to 1.45, were used to determine the crystallization age of this sample. The calculated Concordia Age for the sample was 515 ± 3 Ma, with MSWD = 0.019 and probability = 0.89 (Figure 9B).

Only four analyses were used for the isotopic data of this sample, and the others were discarded from the interpretations because they were outside the quality standards adopted in this work. Model ages for the depleted mantle ranged from 2.93 to 0.59 Ga, and εHf values ranged from −28.39 to 13.09.

5.8. Sample SAIC-10.B

This sample was collected at the same point as sample SAIC-10.A. It was a mesocratic rock with inequigranular texture and fine- to medium-grain size (Figure 10A). The rock was classified as granodiorite and composed essentially of orthoclase, plagioclase, quartz, biotite, titanite, apatite, opaque minerals, and zircon as accessory minerals. On thin slides, apatite crystals with acicular habit could often be observed.

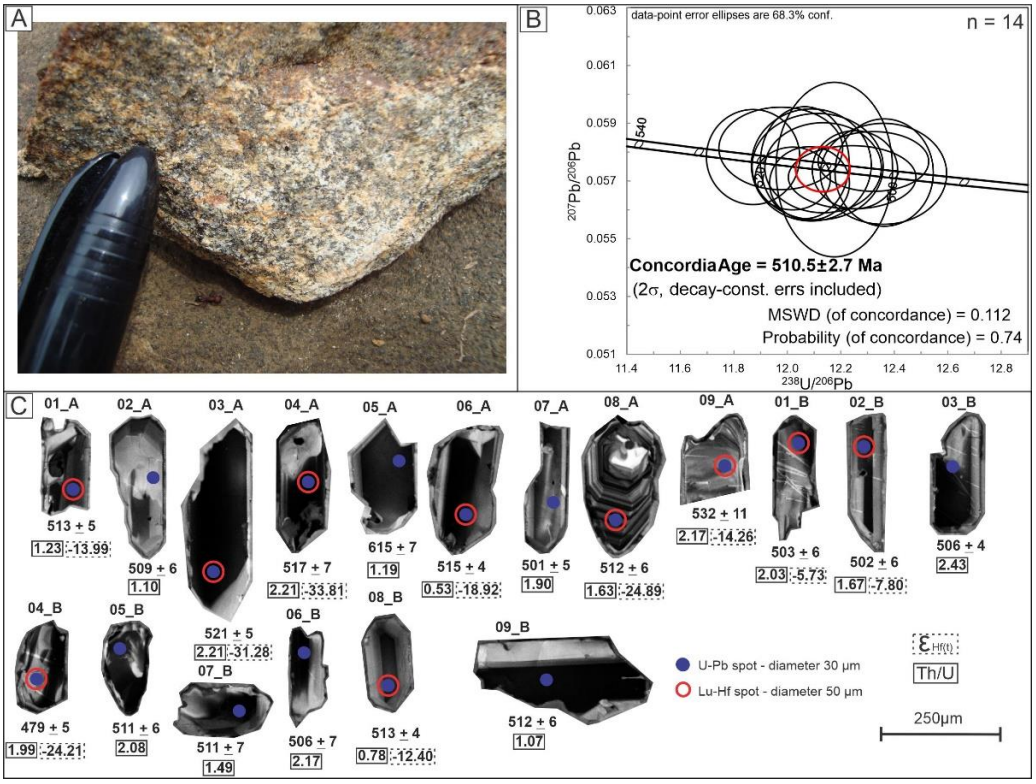

Figure 10. (**A**) A representative sample of SAIC felsic hybrid rock from the point SAIC-10. (**B**) Concord age for the sample SAIC-10B. (**C**) Cathodoluminescence image of the analyzed zircon grains.

The zircon grains from this sample had prismatic and granular habits (grains 05. B and 07. B) with length-to-width ratios of 3:1 and 2:1 (Figure 10C). Analyses of 14 zircon grains (SM.C), with Th/U ratios ranging from 0.53 to 2.43, were used to determine the crystallization age of this sample. The calculated Concordia Age for the sample is 511 ± 3 Ma with MSWD = 0.112 and a probability = 0.74 (Figure 10B). For the isotopic data, eight analyses were used for this sample, and the others were discarded from the interpretations because they were outside the quality standards adopted in this work. Model ages for the depleted mantle ranged from 2.74 to 1.68 Gam, and εHf values ranged from −24.84 to −5.88.

The summary of the geochronological data obtained in this work is presented in Table 1.

Table 1. Summary of the results obtained in this work.

Unit	Sample	Lithotype	Th/U Ratios	U-Pb Age (Ma)	εHf(t)	T_{DM}(Ga)
Ortogneiss Muniz Freire	SAIC-02.A	Metagranite	0.16 to 0.99	595 ± 4	−18.01 to 0.30	2.60 to 1.40
Ortogneiss Muniz Freire	SAIC-13	Metagranite	0.66 to 1.33	595 ± 6	−16.32 to 8.08	2.37 to 0.99
SAIC	SAIC-06.A	Gabronorite	0.57 to 1.94	501 ± 4	−31.45 to −8.46	3.09 to 1.83
SAIC	SAIC-07.A	Quartz diorite	1.21 to 2.43	501 ± 3	−31.34 to 12.44	3.09 to 0.64
SAIC	SAIC-09	Quartz diorite	1.86 to 2.37	510 ± 6	−25.08 to 6.77	2.77 to 0.95
SAIC	SAIC-12	Alkali-feldspar granite	0.88 to 1.73	502 ± 5	−35.28 to −24.25	3.32 to 2.71
SAIC	SAIC-10.A	Monzogranite	0.75 to 1.45	515 ± 3	−28.39 to 13.09	2.93 to 0.59
SAIC	SAIC10.B	Granodiorite	0.53 to 2.43	511 ± 3	−24.84 to −5.88	2.74 to 1.68

6. Discussion

De Campos' work suggests that the main mechanisms of magmatic differentiation were physical dispersion (mingling) and chemical diffusion (mixing), which gave rise to hybrid compositions in the SAIC [22]. On the other hand, Zanon and his collaborators consider that the evolution of the SAIC is associated only with the processes of magma's physical dispersion (mingling) [23]. Despite the discussion between mixing and mingling,

the fact is that magma originating from different sources (crust and mantle) is present in the SAIC, and the hybridization process between the different magmas is a characteristic feature of the SAIC [16–18,45]. The presence of magmas derived from the mantle and crust is commonly reported in the literature for magmatic bodies associated with the post-collisional stage [50–55].

The bimodal behavior between crustal and mantle magmas for post-collisional magmatism is not observed in all AROS. This magmatic bimodality is mainly observed in the bodies of the G5 super suite in the transition zone between the Araçuaí and Ribeira orogens [10]. The presence of mantle components is restricted in the post-collision units of the northern sector of the Araçuaí orogen and the segment of the Ribeira orogen [10,12,39,40,45,56,57].

Despite the extensive work carried out at the SAIC, it is still questioned whether the rocks of this intrusive complex are products of the hybridization of endmembers and, if so, whether such endmembers would be represented in the outcrops of the SAIC [22]. Among the outcrops/samples studied in this work, the sample SAIC-12 (Alkali-feldspar granite) appears to be a good candidate for one of the end members of the mixture that gave rise to the SAIC, as it does not present any textural, structural, and mineralogical characteristics. That indicates some process of magma mixing. Rocks like alkali-feldspar granite, described in this work, were observed by Zanon and his collaborators [21,23]. Therefore, the first window for future studies is to detail the mineralogical and lithogeochemical characteristics of alkali-feldspar granite to test it as one of the uncontaminated endmembers.

The U-Pb ages presented in this work do not differ from those presented previously for SAIC (Figure 11) and the Rio Doce Magmatic Arc rocks. They show that the different magmas present in SAIC crystallized simultaneously [20,25,58]. Although there are many crystallization ages for SAIC, those data are concentrated in the SW lobe (Figure 2). Therefore, a second window for future work opens: obtaining U-Pb ages for the NE lobe and comparing them with the recently proposed model based on magnetic anisotropy data, which considers that the two lobes could not have crystallized simultaneously [15,25,59].

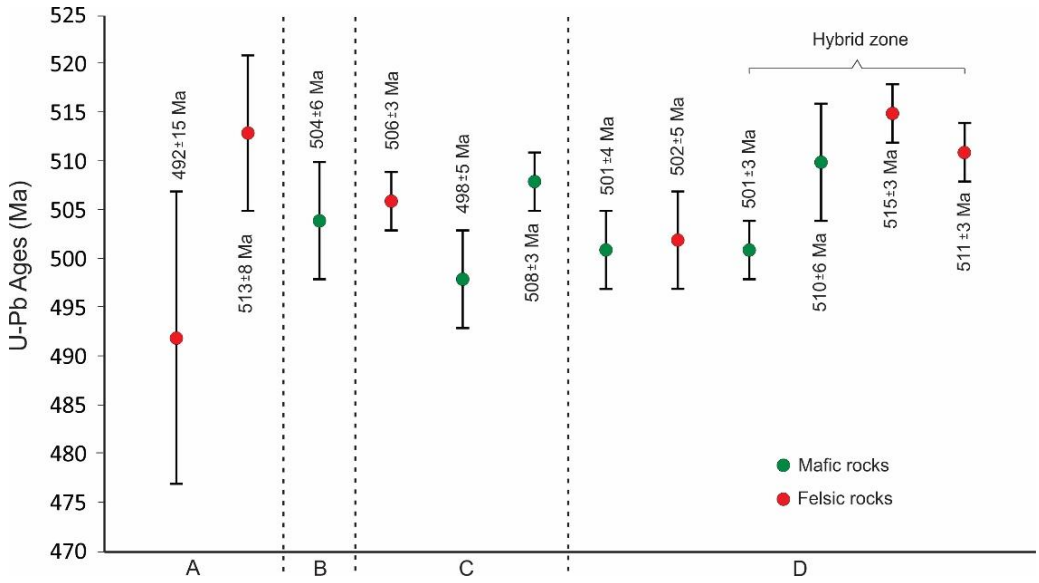

Figure 11. U–Pb ages presented for the Santa Angelica Intrusive Complex. A—[11]—ID-TIMS; B—[58]—LA-ICP-MS; C—[22]—Shrimp; D—This work—LA-ICP-MS.

The SAIC $^{206}Pb/^{207}Pb$ age histogram suggests three age peaks (Figure 12):

(1) The oldest point at 537 ± 5 Ma corresponds to 22% of the ages. That age corresponds to the end of the syn-collisional stage of the Araçuaí orogen [38,60,61]. No large igneous bodies are formed during the syn-collisional stage in the SAIC region. However, intense migmatization of rocks is described in the region [7]. The lowest limit for SAIC crystallization was considered ca. 513 Ma, though the age distribution of zircon

grains suggests that this limit is older. Another possibility is that older ages are associated with the migmatization process during the syn-collisional stage.

(2) The 510 ± 5 Ma intermediate point corresponds to 56% of the ages. Given the amount of grains with ages close to that peak, the age of 510 Ma can be considered the apex of magmatism in SAIC.

(3) The youngest point at 488 ± 7 Ma corresponds to 22% of the ages. That age peak is close to the age limit of the post-collisional stage of the Araçuaí orogen. However, some magmatic activity was still recorded in zircon grains aged approximately 460 Ma (Figure 12) [38,60,61].

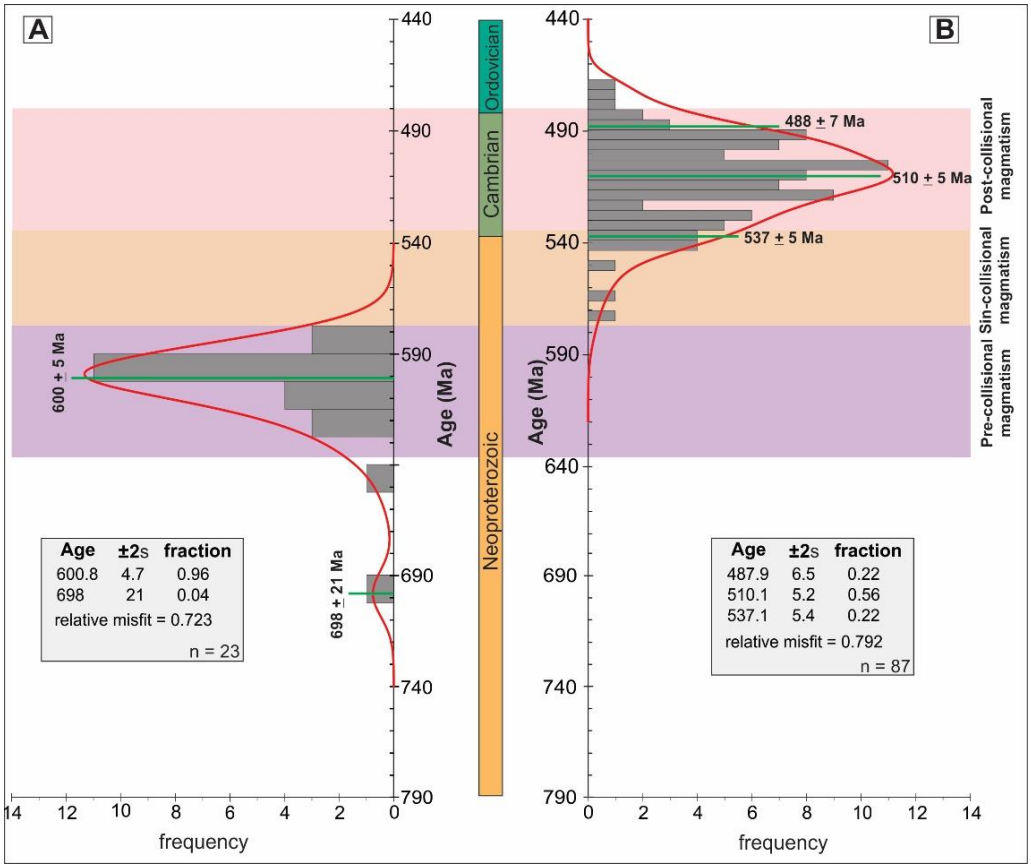

Figure 12. Histograms with the ages obtained for the Muniz Freire orthogneiss in samples: (**A**) SAIC-02 and SAIC-13 and; (**B**) for the ages obtained in samples SAIC-06.A, SAIC-07.A, SAIC-09, SAIC-10.A, SAIC-10.B, SAIC-12. The age intervals of the pre-, sin and post-collisional stages of the Araçuaí orogen [37] were plotted for comparison with the ages obtained in this work.

The ages obtained for the Muniz Freire orthogneiss (595 ± 4 Ma and 595 ± 6 Ma) are in agreement with the age range of the Rio Doce magmatic arc (ca. 632 Ma to ca. 570 Ma) [7]. Similar ages were obtained for the Plutons Guarataia (576 ± 9 Ma), Chaves (599 ± 15 Ma), Brasilândia (581 ± 11 Ma), Muriaé batholith (620 to 592 Ma), Conceição da Boa Vista stocks (586 ± 7 Ma) and Serra do Valentin (605 ± 8 Ma), São Divino suites (592 ± 7 Ma and 603 ± 4 Ma) and orthoderived rocks from the Alegre—ES region (604 ± 3 Ma, 595 ± Ma and 586 ± 5 Ma) [7,62,63].

The age histogram of the Muniz Freire orthogneiss (Figure 12) shows two age peaks (698 ± 21 Ma and 600 ± 5 Ma). The oldest peak is within the age range described for stage 1 development of the Rio Doce magmatic arc, which represents the subduction of an oceanic plate with the generation of rocks related to the magmatic arc [41]. The most recent peak corresponds to the age range of what has been described as stage 3 of the development of

the Rio Doce magmatic arc, which marks the beginning of the collision and the peak of the generation of calc-alkaline granitoids [41].

The isotopic data obtained in this work for the SAIC differ from other post-collision bodies of AROS. The Afonso Cláudio Intrusive Complex (ACIC) presents εHf values in zircon grains ranging from −11.78 to 10.41 (Figure 13) and model ages for the depleted mantle ranging from 1.79 to 1.72 Ga [39]. For the Sana granite, εHf values in zircon grains ranged from −15.54 to −6.54 (Figure 13), and model ages (TDM) ranged from 2.22 to 1.69 Ga [13]. The Mestre Álvaro and Vitória plutons presented εHf values in zircon grains varying from −10.30 to −7.40 and from −8.80 to −0.70, respectively (Figure 13) [41]. The Arecê-Pedra Azul Intrusive Complex presented εHf values ranging from −23.80 to −18.60 (Figure 13) and Paleoproterozoic model ages [41]. Finally, only the Forno Grande Intrusive Complex has an isotopic signature similar to the SAIC, with εHf ranging from −36.62 to +12.70 (Figure 13) and model ages between 3.32 and 0.59 Ga [41].

The SAIC's isotopic signature suggests that at least three magmatic sources were present, namely: a mantle source with positive εHf values; a crustal source with negative εHf values and Meso to Neoproterozoic model ages; and a crustal source with highly negative εHf values and Paleoproterozoic and Archean model ages. The crustal source that presents Paleoproterozoic and Archean model ages has similarities with the signatures of the Caparaó suite, which was associated with the Juiz de Fora Complex (Figure 13) [62,64]. The crustal source that presents Meso to Neoproterozoic model ages has affinities with the isotopic signatures found in the paraderived rocks of the Bom Jesus do Itabapoana Group, the Nova Venécia Complex, and the Rio Doce magmatic arc (Figure 13) [41,44].

The Hf isotopic data for the Muniz Freire orthogneiss point to at least two components, one crustal and the other mantle. The crustal component supports the hypothesis that the Rio Doce Magmatic Arc was formed in a confined tectonic environment, with a thick continental crust and the resurgent mantle acting more as a heat source than a magma source [7]. However, the isotopic data presented in this work points to a juvenile component for this segment of the magmatic arc, with positive epsilon Hf values ranging from 0.30 to 8.80 and model ages (TDM) between 1.40 and 0.99 Ga, which are similar to the juvenile signatures of the Rio Negro Magmatic Arc [6].

The petrogenetic model presented for the G5 super suite suggests that, from the Paleocene opening stage until the collision, the sublithospheric mantle was of incompatible elements through subduction and associated metasomatism seems to be a rule for post-collisional magmatism in the various known moving ranges [10,65]. The positive values of εHf obtained for the host rocks and the model ages varying from 1.40 to 0.99 Ga suggest that some mantle magmatic activity was already active in the embryonic stage of the Rio Doce Magmatic Arc (pre-collisional stage). The decompression process caused by the collapse of the orogenic system, associated with the presence of a large fault zone that crosses the sublithospheric mantle, contributed to the supply of heat and additional flow of volatiles to facilitate crustal anatexis [10]. Crustal lineaments, such as deep fault zones, provide a preferential path for the emplacement of magma in the crust. An example of similar placement exerted by deep structures in the magmatic ascent of the locus versus the trivial role played by overburden geology is the Coastal Batholith of Peru [66–69].

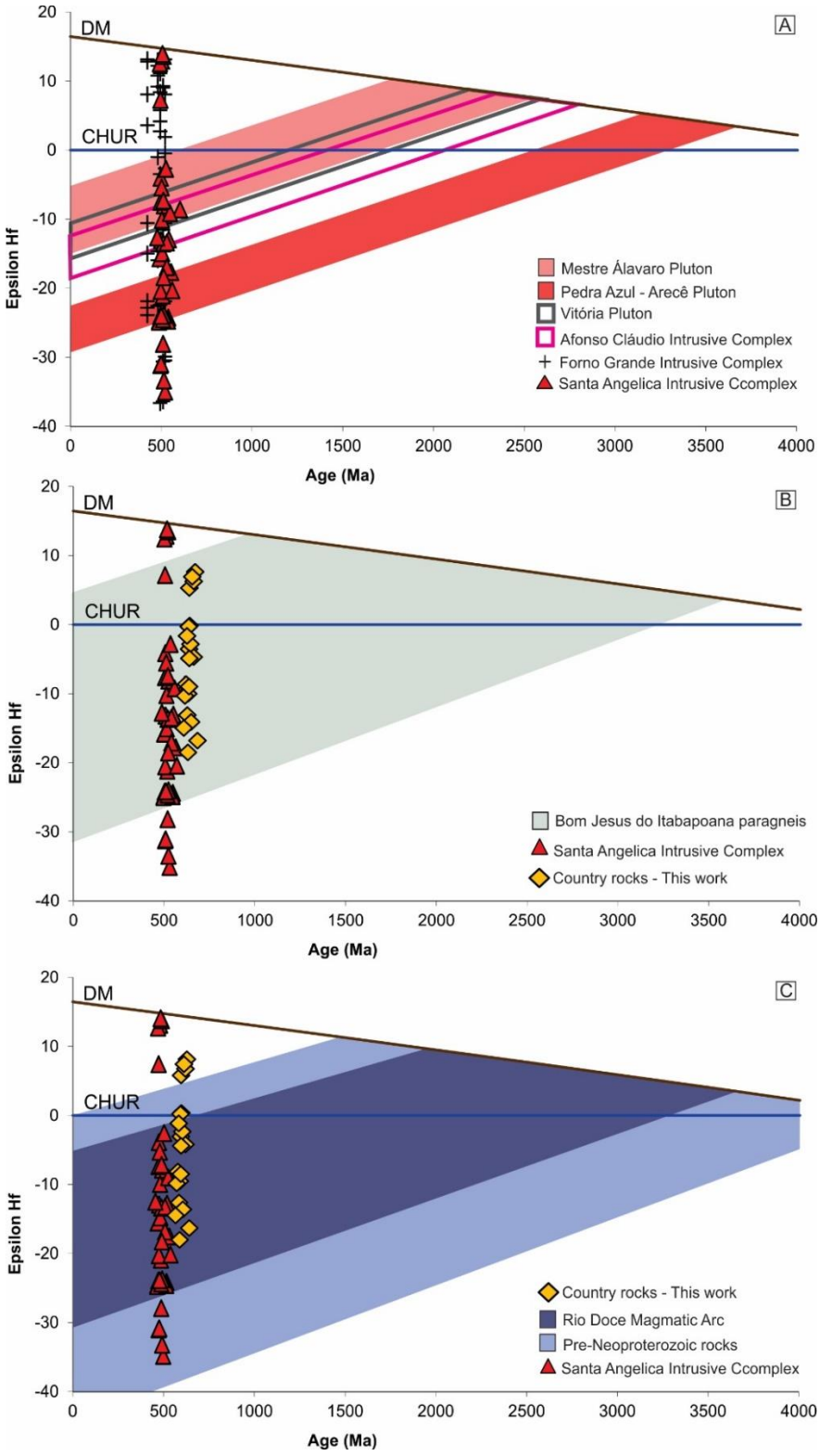

Figure 13. Hf isotopic evolution diagrams from chondritic reservoirs (CHUR) and the depleted mantle (DM). (**A**) presents the εHf data from this work (for SAIC rocks) and data compiled from the work of [39–41] for the G5 supersuite units. (**B**) presents the εHf values of this work for the SAIC and surrounding rocks (Muniz Freire orthogneiss), compared with the εHf data obtained for the Bom Jesus do Itabapoana paragneisse, compiled from [44] and [32]. (**C**) shows the εHf values of this work for the SAIC and surrounding rocks (Muniz Freire orthogneiss), compared to the rocks of the Rio Negro Magmatic Arc [7,34], and to the rocks of the Rhyacian-Orosian basement, whose data were compiled from [32,65].

7. Conclusions

The geochronological data obtained for the country rocks of the SAIC (595 ± 4 Ma and 959 ± 6 Ma), which represent the Rio Doce magmatic arc in the region, agree with the continental collision stage recorded for this magmatic arc, being the peak period for the generation of calc-alkaline granitoids. The oldest grains, which document an age peak of 698 Ma, mark the beginning of the subduction process; that is, the set of ages obtained for the Muniz Freire orthogneiss records the evolutionary history of the magmatic arc. About 75% of the isotopic data (Lu-Hf) support the hypothesis that the Rio Doce magmatic arc developed in a continental environment. However, the presence of a juvenile component was identified in a smaller set of isotopic data, suggesting that some mantle component was also present during the evolution of the magmatic arc.

The ages obtained for the SAIC do not show significant variation between acidic and basic rocks, which confirms that the magmas that gave rise to this intrusive complex are cogenetic. The set of ages obtained allowed us to define three age peaks for the development of magmatism in the SAIC: (1) the first peak of 537 ± 5, which corresponds to the period of crustal anatexis and possibly marks the beginning of the generation of larger volumes of magmas of crustal origin; (2) the 510 ± 5 Ma peak marks the magmatic peak in the SAIC and corresponds to the post-collisional magmatic peak of the Araçuaí–Ribeira Orogenic System; and (3) the youngest peak of 488 ± 7 Ma marks the limit of magma generation at SAIC. However, despite the geochronological robustness, only the SW lobe of the SAIC has age information, which opens an opportunity for future geochronological studies in the NE lobe.

The Hf isotopic data confirm the petrogenetic model that suggests the hybridization of mantle magmas and crustal origins. The positive values of εHf demonstrate the mantle component in conjunction with the ages of the Neoproterozoic model. The placement of these mantle magmas at higher crustal levels possibly occurred from deep fault zones that reach the lithospheric mantle. Regarding the crustal source, the isotopic data point to at least two distinct sources that contributed as sources and contaminants to the granitic magmatism of the SAIC. The highly negative εHf values (≤ -25) in the Archean ages model suggest that the lower crust, represented by the Caparaó suite (Juiz de Fora Complex), is one of the crustal components of the SAIC. Another possible crustal source/contaminant is the middle/upper crust, represented by the rocks of the Rio Doce magmatic arc and the paragneisses of the Bom Jesus do Itabapoana group. At least one of the uncontaminated end members of the SAIC may have been found in this work, namely alkali-feldspar granite.

Supplementary Materials: The following are available online at https://www.mdpi.com/article/10.3390/min12111378/s1, File S1: Supplementary material (A–D).

Author Contributions: Conceptualization: G.L.P. and M.C.G.; methodology: G.L.P. and M.C.G.; formal analysis: G.L.P.; investigation: G.L.P. and M.C.G.; resources: G.L.P., M.C.G. and M.V.A.M.; writing—review and editing: G.L.P., M.V.A.M., E.B.d.M.J. and F.A.T.; visualization: G.L.P., M.V.A.M., E.B.d.M.J. and F.A.T. All authors have read and agreed to the published version of the manuscript.

Funding: The authors would like to thank the Conselho Nacional de Desenvolvimento Científico e Tecnológico of Brazil, CNPq (project processes #302676/2019-8 to MVAM; and processes #301470/2016-2 to MCG) and Fundação Carlos Chagas Filho de Amparo à Pesquisa do Estado do Rio de Janeiro, FAPERJ (project processes: E-26/202.927/2019 to MVAM; E-26/202.843/2017 to MCG; E-26/203.112/2016 and E-26/204.531/2021 to GLP) Brazil, for financial support.

Data Availability Statement: Not Applicable.

Conflicts of Interest: The authors declare no conflict of interest.

References

1. Silva, M.E.; Vauchez, A.; Fossen, H.; Cavalcante, G.C.G.; Xavier, B.C. Connecting the Araçuaí and Ribeira belts (SE–Brazil): Progressive transition from contractional to transpressive strain regime during the Brasiliano orogeny. *J. S. Am. Earth Sci.* **2018**, *86*, 127–139. [CrossRef]
2. Almeida, F.F.M. O Cráton do São Francisco. *Rev. Bras. Geociênc.* **1977**, *7*, 349–364.
3. Soares, C.; Queiroga, G.; Pedrosa-Soares, A.; Gouvêa, L.P.; Valeriano, C.M.; Melo, M.G.; Marques, R.; Delicio, R. The Ediacaran Rio Doce magmatic arc in the Araçuaí–Ribeira boundary sector, southeast Brazil: Lithochemistry and isotopic (Sm–Nd and Sr) signatures. *J. S. Am. Earth Sci.* **2020**, *104*, 102880. [CrossRef]
4. Pedrosa-Soares, A.C.; Wiedemann-Leonardos, C.M. Evolution of the Araçuaí belt and its connection to the Ribeira belt, eastern Brazil. In *Tectonic Evolution of South America*; Cordani, U., Milani, E., Thomaz-Filho, A., Campos, D.A., Eds.; Sociedade Brasileira de Geologia: São Paulo, Brazil, 2000; pp. 265–285.
5. Pedrosa-Soares, A.C.; Noce, C.M.; Wiedemann, C.M.; Pinto, C.P. The Araçuaí- West-Congo Orogen in Brazil: An over-view of a confined orogen formed during Gondwanaland assembly. *Precambrian Res.* **2001**, *110*, 307–323. [CrossRef]
6. Heilbron, M.; Valeriano, C.; Peixoto, C.; Tupinambá, M.; Neubauer, F.; Dussin, I.; Corrales, F.; Bruno, H.; Lobato, M.; Almeida, J.C. Neoproterozoic magmatic arc systems of the central Ribeira belt, SE-Brazil, in the context of the West-Gondwana pre-collisional history: A review. *J. S. Am. Earth Sci.* **2020**, *103*, 102710. [CrossRef]
7. Tedeschi, M.; Novo, T.; Pedrosa-Soares, A.; Dussin, I.; Tassinari, C.; Silva, L.C.; Dantas, E. The Ediacaran Rio Doce magmatic arc revisited (Araçuaí-Ribeira orogenic system, SE Brazil). *J. S. Am. Earth Sci.* **2016**, *68*, 167–186. [CrossRef]
8. Santiago, R.; Caxito, F.A.; Pedrosa-Soares, A.C.; Neves, M.A.; Calegari, S.S.; Lana, C. Detrital zircon U–Pb and Lu–Hf constraints on the age, provenance and tectonic setting of arc-related high-grade units of the transition zone of the Araçuaí and Ribeira orogens (SE Brazil). *J. S. Am. Earth Sci.* **2022**, *116*, 103861. [CrossRef]
9. Heilbron, M.; Pedrosa-Soares, A.C.; Campos Neto, M.C.; Silva, L.C.; Truow, R.A.J.; Janasi, V.A. *Geologia do Continente Sul-Americano: Evolução da obra de Fernando Flávio Marques de Almeida*; Mantesso-Neto, V., Bartoreli, A., Carneiro, C.D.R., Brito-Neves, B.B., Eds.; Beca: São Paulo, Brazil, 2004; pp. 203–234.
10. De Campos, C.P.; Medeiros, S.R.; Mendes, J.C.; Pedrosa-Soares, A.C.; Dussin, I.; Ludka, I.P.; Dantas, E.L. Cambro-ordovician magmatism in the Araçuaí belt (SE Brazil): Snapshots from a post-collisional event. *J. S. Am. Earth Sci.* **2016**, *68*, 248–268. [CrossRef]
11. Valeriano, C.M.; Mendes, J.C.; Tupinambá, M.; Bongiolo, E.; Heilbron, M.; Junho, M.C.B. Cambro-Ordovician post-collisional granites of the Ribeira Belt, SE-Brazil: A case of terminal magmatism of a hot orogen. *J. S. Am. Earth Sci.* **2016**, *68*, 416–428. [CrossRef]
12. Valeriano, C.M.; Tupinambá, M.; Simonetti, A.; Heilbron, M.; Almeida, J.C.H.; Eiraldo, L.G. U-Pb LA-MC-ICPMS geo-chronology of Cambro-Ordovician post-collisional granites of the Ribeira belt, southeast Brazil: Terminal Brasiliano magmatism in central Gondwana supercontinent. *J. S. Am. Earth Sci.* **2011**, *32*, 416–428. [CrossRef]
13. Potratz, G.L.; Geraldes, M.C.; Martins, M.V.A.; de Almeida, B.S. Sana Granite, a post-collisional S-type magmatic suite of the Ribeira Belt (Rio de Janeiro, SE Brazil). *Lithos* **2021**, *388–389*, 106077. [CrossRef]
14. De Campos, C.P.; Mendes, J.C.; Ludka, I.P.; Medeiros, S.R.; Moura, J.C.; Wallfass, C. A review of the Brasilian magmatism in southern Espírito Santo, Brazil, with emphasis on post-collisional magmatism. *J. Virtual Explor.* **2004**, *17*, 35. [CrossRef]
15. Souza-Junior, G.F.; Trindade, R.I.F.; Temporim, F.A.; Bellon, U.D.; Gouvêa, L.P.; Soares, C.C.; Amaral, C.A.D.; Louro, V. Imaging the roots of a post-collisional pluton: Implications for the voluminous Cambrian magmatism in the Araçuaí orogen (Brazil). *Tectonophysics* **2021**, *821*, 229146. [CrossRef]
16. Bayer, P.; Schimidt-Thomé, R.; Weber-Diefenbach, K.; Horn, H.A. Complex concentric granitoid intrusions in the coastal mobile belt, Espírito Santo, Brazil: The Santa Angélica Pluton—An axample. *Geol. Rundsch.* **1987**, *76*, 357–371. Available online: https://link.springer.com/article/10.1007/BF01821080 (accessed on 25 June 2020). [CrossRef]
17. Schmidt-Thomé, R.; Weber-Diefenbach, K. Evidence for frozen-in magma mixing in Brasiliano calc-alkaline intrusions: The Santa Angélica pluton, southern Espírito Santo, Brazil. *Rev. Bras. Geociênc.* **1987**, *17*, 498–506.
18. Wiedemann, C.M.; Penha, M.P.; Schmidt-Thomé, R. Granitoids of Espírito Santo and Rio de Janeiro state (Excursion Guide). SBG. In Proceedings of the International Symposium on Granite and Associated Mineralizations, Salvador, Brazil, 21–23 January 1987.
19. Horn, H.A.; Weber-Diefenbach, K. Geochemical and genetic studies of three inverse zoned intrusive bodies of both alkaline and subalkaline composition in the Aracuaí-Ribeira Mobile Belt (Espírito Santo, Brazil). *Rev. Bras. Geociênc.* **1987**, *17*, 488–497.
20. Söllner, F.; Lammerer, B.; Wiedeman-Leonardos, C.M. Dating the Ribeira Mobile Belt. *Z. Angwandte Geol.* **2000**, *1*, 245–255.
21. Zanon, M.L.; Chaves, A.O.A.; Gabrig, C.V.T. A origem das bordas de mirmequita nos xenocristais de feldspato potássico em rochas máficas e híbridas do Maciço Santa Angélica—ES. *Geonomos* **2012**, *20*, 23–33. [CrossRef]
22. De Campos, C.P. Chaotic flow patterns from a deep plutonic environment: A case study on natural magma mixing. *Pure Appl. Geophys.* **2015**, *172*, 1815–1833. Available online: https://link.springer.com/article/10.1007/s00024-014-0940-6 (accessed on 20 May 2019). [CrossRef]
23. Zanon, M.L.; Chaves, A.O.; Rangel, C.V.G.T.; Gaburu, L.; Pires, C.R. Os aspectos geológicos do Maciço Santa Angélica (ES): Uma nova abordagem. *Braz. J. Geol.* **2015**, *45*, 609–633. [CrossRef]
24. Slaby, E.; De Campos, C.P.; Majzner, K.; Simon, K.; Gros, K.; Moszumanska, I.; Jokubauskas, P. Feldspar megacrysts from the Santa Angélica composite pluton—Formation/transformation path revealed by combined CL, Raman and LA-ICP-MS data. *Lithos* **2017**, *277*, 269–283. [CrossRef]

25. Temporim, F.A.; Trindade, R.I.F.; Tohver, E.; Soares, C.C.; Gouvêa, L.P.; Egydio-Silva, M.; Amaral, C.A.D.; Souza, G.F., Jr. Magnetic Fabric and Geochronology of a Cambrian "Isotropic" Pluton in the Neoproterozoic Araçuaí Orogen. *Tectonics* **2020**, *39*, e2019TC005877. [CrossRef]
26. Alkmin, F.F.; Marshak, S.; Pedrosa-Soares, A.C.; Peres, G.G.; Cruz, S.C.P.; Whittington, A. Kinematic evolution of the Araçuaí-West Congo orogen in Brazil and Africa: Nutcracker tectonics during the Neoproterozoic assembly of Gondwana. *Precambrian Res.* **2006**, *149*, 43–64. [CrossRef]
27. Heilbron, M.; Mohriak, W.U.; Valeriano, C.M.; Milani, E.J.; Almeida, J.; Tupinambá, M. From collision to extension: The roots of the south-eastern continental margin of Brazil. *Geophys. Monogr. Am. Geophys. Union* **2000**, *115*, 1–34.
28. Truow, R.A.J.; Heilbron, M.; Ribeiro, A.; Paciullo, F.V.P.; Valeriano, C.M.; Almeida, J.C.J.; Tupinambá, M. The central segment of the Ribeira Belt. In *Tectonic Evolution of South America*; Cordani, U., Milani, E.J., Eds.; Sociedade Brasileira de Geologia: São Paulo, Brazil, 2000; pp. 287–310.
29. Schmitt, R.D.S.; Trouw, R.; Van Schmus, W.R.; Pimentel, M. Late amalgamation in the central part of Western Gondwana: New geochronological data and the characterization of a Cambrian collision orogeny in the Ribeira Belt (SE Brazil). *Precambrian Res.* **2004**, *46* (Suppl. S1), 37–66. [CrossRef]
30. Tupinambá, M.; Heilbron, M.; Duarte, B.P.; Nogueira, J.R.; Valladares, C.; Almeida, J.; Silva, L.G.E.; Medeiros, S.R.; Almeida, C.G.; Miranda, A.; et al. Geologia da Faixa Ribeira Setentrional: Estado da arte e conexões com a Faixa Araçuaí. *Geonomus* **2007**, *15*, 67–79. [CrossRef]
31. Corrales, F.F.P.; Dussin, I.; Heilbron, M.; Bruno, H.; Bersan, S.; Valeriano, C.M.; Pedrosa-Soares, A.C.; Tedeschi, M. Coeval high Ba-Sr arc-related and OIB Neoproterozoic rocks linking precollisional magmatism of the Ribeira and Araçuaí orogenic belts, SE-Brazil. *Precambrian Res.* **2020**, *337*, 105476. [CrossRef]
32. Degler, R.; Pedrosa-Soares, A.; Dussin, I.; Queiroga, G.; Schulz, B. Contrasting provenance and timing of metamorphism from paragneisses of the Araçuaí-Ribeira orogenic system, Brazil: Hints for Western Gondwana assembly. *Gondwana Res.* **2017**, *51*, 30–50. [CrossRef]
33. Vieira, V.S. Significado do Grupo Rio Doce no Contexto do Orógeno Araçuaí. Ph.D. Thesis, Universidade Federal de Minas Gerais, Belo Horizonte, Brazil, 2007.
34. Gonçalves, L.; Alkmim, F.F.; Pedrosa-Soares, A.C.; Dussin, I.A.; Valeriano, C.M.; Lana, C.; Tedeschi, M. Granites of the intracontinental termination of a magmatic arc: An example from the Ediacaran Araçuaí orogen, southeastern Brazil. *Gondwana Res.* **2016**, *36*, 439–458. [CrossRef]
35. Noce, C.M.; Pedrosa-Soares, A.C.; Silva, L.C.; Armstrong, R.; Piuzana, D. Evolution of polyciclic basement complexes in the Araçuaí Orogen, based on U-Pb SHRIMP data: Implications for Brazil-Africa links in Paleoproterozoic time. *Precambrian Res.* **2007**, *159*, 60–78. [CrossRef]
36. Heilbron, M.; Duarte, B.; Valeriano, C.; Simonetti, A.; Machado, N.; Nogueira, J. Evolution of reworked Paleoproterozoic basement rocks within the Ribeira belt (Neoproterozoic), SE-Brazil, based on U Pb geochronology: Implications for paleogeographic reconstructions of the São Francisco-Congo paleocontinent. *Precambrian Res.* **2010**, *178*, 136–148. [CrossRef]
37. Pedrosa-Soares, A.C.; De Campos, C.P.; Noce, C.M.; Silva, L.C.; Novo, T.; Roncato, J.; Medeiros, S.; Castañeda, C.; Queiroga, G.; Dantas, E.; et al. Late neoproterozoic-cambrian granitic magmatism in the Araçuaí orogen (Brazil), the eastern Brazilian pegmatite province and related mineral resources. *Geol. Soc. Lond. Spec. Publ.* **2011**, *350*, 25–51. [CrossRef]
38. Gradim, C.; Roncato, J.; Pedrosa-Soares, A.C.; Cordani, U.; Dussin, I.; Alkmim, F.F.; Queiroga, G.; Jacobsohn, T.; Silva, L.C.; Babinski, M. The hot back-arc zone of the Araçuaí Orogen, Eastern Brazil: From sedimentation to granite generation. *Braz. J. Genet.* **2014**, *44*, 155–180. [CrossRef]
39. Aranda, R.O.; Horn, A.H.; Medeiros Junior, E.B.; Venturini Junior, R. Geothermobarometry of igneous rocks from Afonso Cláudio intrusive complex (Espírito Santo State, Southeastern Brazil), Araçuaí-West Congo Orogen: Further evidence for deep emplacement levels. *J. S. Am. Earth Sci.* **2020**, *110*, 103016. [CrossRef]
40. Araujo, C.; Pedrosa-Soares, A.; Lana, C.; Dussin, I.; Queiroga, G.; Serrano, P.; Medeiros-Júnior, E. Zircon in emplacement borders of post-collisional plutons compared to country rocks: A study on morphology, internal texture, UeThePb geochronology and Hf isotopes (Araçuaí orogen, SE Brazil). *Lithons* **2020**, *352*, 105252. [CrossRef]
41. Macedo, I.M.L.; Geraldes, M.C.G.; Marques, R.A.; Melo, M.G.; Tavares, A.D.; Martins, M.V.A.; Oliveira, H.C.; Rodrigues, R.D. New clues for magma-mixing processes using petrological and geochronological evidence from the Castelo Intrusive Complex, Araçuaí Orogen (SE Brazil). *J. S. Am. Earth Sci.* **2022**, *115*, 103758. [CrossRef]
42. Da Silva, J.N. *Cachoeiro de Itapemirim, folha SF.24-V-A-V: Escala 1:100.000*; Technical Report for Programa de Levantamentos Geológicos do Brasil; Companhia de Pesquisa de Recursos Minerai: Brasilia, Brazil, 1993; 163p.
43. Signorelli, N. *Afonso Claudio, folha SF.24-V-A-II: Escala 1:100.000*; Technical Report for Programa de Levantamentos Geológicos do Brasil; Companhia de Pesquisa de Recursos Minerai: Brasilia, Brazil, 1993; 153p.
44. Alves, M.I. Metassedimentos do Grupo Andrelândia e Complexo Paraíba do Sul na Região da Zona de Cisalhamento Guaçuí (ES): Idades de Upb/Lu-Hf (LA-ICP-MS) em Zircões Detríticos Para a Análise de Proveniência. Master's Thesis, Universidade do Estado do Rio de Janeiro, Rio de Janeiro, Brazil, 2016.
45. Wiedemann, C.M.; Medeiros, S.R.; Mendes, J.C.; Ludka, I.P.; Costa-de-Moura, J. Architecture of Late Orogenic Plutons in the Aracuaí-Ribeira Folded Belt, Southeast Brazil. *Gondwana Res.* **2002**, *19*, 381–399. [CrossRef]

46. Torres, L.F. *Petrografia e Geoquímica de Plútons Zonados do Sul do Espírito Santo*; Monografia, Universidade Federal do Espírito Santo: Vitória, Brazil, 2013.
47. Corfu, F.; Hanchar, J.M.; Hoskin, P.W.O.; Kinny, P. Atlas of zircon textures. *Rev. Mineral. Geochem.* **2003**, *53*, 469–500. [CrossRef]
48. Jackson, S.E.; Pearson, N.J.; Griffin, W.L.; Belousova, E.A. The application of laser ablation–inductively coupled plasma–mass spectrometry to in situ U–Pb zircon geochronology. *Chem. Geol.* **2004**, *211*, 47–69. [CrossRef]
49. Ludwig, K.R. *User's manual for Isoplot 3.75: A geochronological toolkit for Microsoft Excel*; Special Publication 5; Berkeley Geochronological Center: Berkeley, CA, USA, 2012.
50. Alves, M.I.; Almeida, B.S.; Cardoso, L.M.C.; Santos, A.C.; Appi, C.; Bertotti, A.L.; Chemale, F.; Tavares, A.D., Jr.; Martins, M.V.A.; Geraldes, M.C. Isotopic composition of Lu, Hf, and Yb in GJ-01, 91,500, and Mud Tank reference materials measured by LA-ICP-MS: Application of the Lu-Hf geochronology in zircon. *J. Sediment. Environ.* **2019**, *4*, 220–248. [CrossRef]
51. Harris, N.B.W.; Pearce, A.J.; Tindle, A.G. Gepchemical characteristics of collision-zone magmatism. *Geol. Soc. Lond. Spec. Publ.* **1986**, *19*, 67–81. [CrossRef]
52. Liégeois, J.P.; Navez, J.; Hertogen, J.; Black, R. Contrasting origin of post-collisional high-K calc-alkaline and shoshonitic versus alkaline and peralkaline granitoids: The use of sliding normalization. *Lithos* **1998**, *41*, 1–28. [CrossRef]
53. Fan, W.M.; Guo, F.; Wang, Y.J.; Zhang, M. Post-orogenic bimodal volcanism along the Sulu Orogenic Belt in Eastern China. *Phys. Chem. Earth* **2001**, *26*, 133–146. [CrossRef]
54. Chung, S.L.; Chu, M.F.; Zhang, Y.; Xie, Y.; Lo, C.H.; Lee, T.Y.; Lan, C.Y.; Li, X.; Zhang, Q.; Wang, Y. Tibetan tectonic evolution inferred from spatial and temporal variations in post-collisonal magmatism. *Earth Sci. Rev.* **2005**, *68*, 173–196. [CrossRef]
55. Finger, F.; Gerdes, A.; Rene, M.; Riegler, G. The Saxo-Danubian Granite Belt: Magmatic response to postcollisional delamination of mantle lithosphere below the southwestern sector of the Bohemian Massif (Variscan orogen). *Geol. Carpath.* **2009**, *3*, 205–212. [CrossRef]
56. Potratz, G.L.; Valeriano, C.M. Petrografia e litogeoquímica do granito Itaoca, município de Campos dos Goytacazes, RJ: O representante mais jovem do magmatismo pós-colisional da Faixa Ribeira. *Geonomus* **2017**, *25*, 1–13. [CrossRef]
57. Bione, F.R.A.; Bongiolo, E.M.; Mendes, J.C.; Roland, C.L. Geochemistry, Sm-Nd isotopes and SHRIMP U-Pb geochronology of the Morro do Coco Granite (RJ, Brazil): Another piece of the post-collisional magmatism of the Ribeira Belt. *Braz. J. Geol.* **2019**, *49*, 1–19. [CrossRef]
58. Santiago, R.; Caxito, F.A.; Neves, M.A.; Dantas, E.L.; Medeiros Júnior, E.B.; Queiroga, G.N. Two generations of mafic dyke swarms in the Southeastern Brazilian coast: Reactivation of structural lineaments during the gravitational collapse of the Araçuaí-Ribeira Orogen (500 Ma) and West Gondwana breakup (140 Ma). *Precambrian Res.* **2020**, *340*, 105344. [CrossRef]
59. Temporim, F.A.; Bellon, U.D.; Domeier, M.; Trindade, R.I.F.; D'Agrella-Filho, M.S.; Tohver, E. Constraining the Cambrian drift of Gondwana with new paleomagnetic data from post-collisional plutons of the Araçuaí orogen, SE Brazil. *Precambrian Res.* **2021**, *359*, 106212. [CrossRef]
60. Pedrosa-Soares, A.C.; Alkmim, F.F.; Tack, L.; Noce, C.M.; Babinski, M.; Silva, L.C.; Martins-Neto, M.A. Similarities and differences between the Brazilian and African counterparts of the Neoproterozoic Araçuaí–West Congo orogen. *Geol. Soc. Lond. Spec. Publ.* **2008**, *294*, 153–172. [CrossRef]
61. Bento dos Santos, T.; Munhá, J.; Tassinari, C.; Fonseca, P.; Dias Neto, C. Thermochronology of central Ribeira Fold Belt, SE Brazil: Petrological and geochronological evidence for high temperature maintenance during western Gondwana amalgamation. *Precambrian Res.* **2010**, *180*, 285–298. [CrossRef]
62. Novo, T.A.; Pedrosa-Soares, A.C.; Noce, C.M.; Alkmim, F.F.; Dussin, A.I. Rochas charnockíticas do sudeste de Minas Gerais: A raiz granulítica do arco magmático do Orógeno Araçuaí. *Rev. Bras. Geociênc.* **2010**, *40*, 573–592. [CrossRef]
63. Gouvea, L.P.; Medeiros, S.R.; Mendes, J.C.; Soares, C.; Marques, R.; Melo, M. Magmatic activity period and estimation of P-T metamorphic conditions of pre-collisional opx-metatonalite from Araçuaí-Ribeira orogens boundary, SE Brazil. *J. S. Am. Earth Sci.* **2020**, *99*, 102506. [CrossRef]
64. Gualandi, T.F.; Alves, M.I.; Potratz, G.L.; Silva, L.F.R.; Rodrigues, S.W.O.; Martins, M.V.A.; Geraldes, M.C. The Serra do Caparaó Complex, Mantiqueira Province, Brazil, revisited: Metamorphic age constraints by U-Pb na Lu-Hf method in zircon by LA-ICP-MS. *J. Geol. Surv. Braz.* **2022**, *5*, 49–80. [CrossRef]
65. Couzinié, S.; Laurent, O.; Moyen, J.F.; Zeh, A.; Bouilhol, P.; Villaros, A. Post-collisional magmatism: Crustal growth not identified by zircon Hf–O isotopes. *Earth Planet. Sci. Lett.* **2016**, *456*, 182–195. [CrossRef]
66. Pitcher, W.S.; Bussel, M.A. Structural control of batholithic emplacement in Peru: A review. *J. Geol. Soc.* **1977**, *133*, 249–256. [CrossRef]
67. Grocott, J.; Arévalo, C.; Welkner, D.; Cruden, A. Fault-assisted vertical pluton growth: Coastal cordillera, north Chilean Andes. *J. Geol. Soc.* **2009**, *166*, 295–301. [CrossRef]
68. Pitcher, W.S. The nature, ascent, and emplacement of granitic magrnas. *J. Geol. Soc. Lond.* **1979**, *163*, 627–662. [CrossRef]
69. Seymour, N.M.; Singleton, J.S.; Mavor, S.P.; Gomila, R.; Stockli, D.F.; Heuser, G.; Arancibia, G. The relationship between magmatism and deformation along the intra-arc strike-slip Atacama fault system, northern Chile. *Tectonics* **2020**, *39*, e2019TC005702. [CrossRef]